HHS Public Access

Author manuscript

Sci Transl Med. Author manuscript; available in PMC 2023 May 05.

Published in final edited form as:

Sci Transl Med. 2022 March 23; 14(637): eabl7634. doi:10.1126/scitranslmed.abl7634.

The niacin receptor HCAR2 modulates microglial response and limits disease progression in a mouse model of Alzheimer's disease

Miguel Moutinho[1,2], **Shweta S. Puntambekar**[1,3], **Andy P. Tsai**[1], **Israel Coronel**[1,2], **Peter B. Lin**[1], **Brad T. Casali**[4,†], **Pablo Martinez**[1,2], **Adrian L. Oblak**[1,5], **Cristian A. Lasagna-Reeves**[1,2], **Bruce T. Lamb**[1,3], **Gary E. Landreth**[1,2,*]

[1]Stark Neurosciences Research Institute, Indiana University School of Medicine, Indianapolis, IN 46202, USA

[2]Department of Anatomy, Cell Biology and Physiology, Indiana University School of Medicine, Indianapolis, IN 46202, USA

[3]Department of Medical and Molecular Genetics, Indiana University School of Medicine, Indianapolis, IN 46202, USA

[4]Department of Neurosciences, School of Medicine, Case Western Reserve University, Cleveland, OH 44106, USA

[5]Department of Radiology and Imaging Sciences, Indiana University School of Medicine, Indianapolis, IN 46202, USA

Abstract

[*]Corresponding author. glandret@iu.edu.

[†]Present address: Department of Pharmaceutical Sciences, College of Pharmacy, Northeast Ohio Medical University, Rootstown, OH 44272, USA.

Author contributions: M.M. and G.E.L. conceived the study and designed the experiments. M.M. maintained the mouse lines used in this study; performed Niaspan treatments; collected and processed mouse samples; conducted and analyzed qPCR, IHC, and behavioral experiment analysis; conducted experiments with primary cultures of microglia; and analyzed transcriptomic, NanoString, and MSD data. S.S.P. assisted with the design of flow cytometry experiments, conducted the flow cytometry experiments and their analysis, and assisted with Niaspan treatments. A.P.T. performed and analyzed qPCR and behavioral experiments and assisted with Niaspan treatments and primary cultures of microglia. I.C. performed Niaspan treatments and processed samples for CPAC analysis, maintained mouse lines, and performed experiments with primary cultures of microglia. P.B.L. conducted the NanoString and MSD experiments. B.T.C. conducted the Plexxikon treatments and collected and processed the samples. P.M. assisted with the IHC of human tissue and processed all human samples for qPCR. M.M., S.S.P., A.L.O., C.A.L.-R., B.T.L., and G.E.L. interpreted and discussed the results. M.M. and G.E.L. wrote the manuscript with critical revisions from S.S.P., A.L.O., C.A.L.-R., and B.T.L. All authors read and approved the manuscript.

Competing interests: The authors declare that they have no competing interests.

SUPPLEMENTARY MATERIALS

www.science.org/doi/10.1126/scitranslmed.abl7634

Supplementary material and methods

Figs. S1 to S6

Tables S1 and S2

Data files S1 and S2

MDAR Reproducibility Checklist

References (78–82)

View/request a protocol for this paper from Bio-protocol.

Increased dietary intake of niacin has been correlated with reduced risk of Alzheimer's disease (AD). Niacin serves as a high-affinity ligand for the receptor HCAR2 (GPR109A). In the brain, HCAR2 is expressed selectively by microglia and is robustly induced by amyloid pathology in AD. The genetic inactivation of *Hcar2* in 5xFAD mice, a model of AD, results in impairment of the microglial response to amyloid deposition, including deficits in gene expression, proliferation, envelopment of amyloid plaques, and uptake of amyloid-β (Aβ), ultimately leading to exacerbation of amyloid burden, neuronal loss, and cognitive deficits. In contrast, activation of HCAR2 with an FDA-approved formulation of niacin (Niaspan) in 5xFAD mice leads to reduced plaque burden and neuronal dystrophy, attenuation of neuronal loss, and rescue of working memory deficits. These data provide direct evidence that HCAR2 is required for an efficient and neuroprotective response of microglia to amyloid pathology. Administration of Niaspan potentiates the HCAR2-mediated microglial protective response and consequently attenuates amyloid-induced pathology, suggesting that its use may be a promising therapeutic approach to AD that specifically targets the neuroimmune response.

INTRODUCTION

Alzheimer's disease (AD) is the most common form of dementia for which there is no effective treatment. Mounting evidence suggests that the accumulation and aggregation of amyloid-β (Aβ) is a key initiating factor in a cascade of events that lead to AD (1). The AD brain is typified by a robust microglial immune response triggered by Aβ accumulation (2). Furthermore, genetic studies have linked many immune genes subserving this microglial response to the risk of AD (3, 4). Although microglia have emerged as an important player in AD pathogenesis and progression, the role of these cells in disease is complex and still not fully understood.

Increased dietary intake of niacin (nicotinic acid) has been associated with improved cognitive performance (5) and reduced risk of age-associated cognitive decline and AD (6). Niacin is obtained principally through diet and is able to cross the blood-brain barrier (7), as evidenced by its detection in the mouse brain and human cerebrospinal fluid (8, 9). Thus, we postulated that the actions of niacin within the brain may be of therapeutic utility for AD. In the brain, it is unlikely that niacin acts through its canonical role as precursor of nicotinamide adenine dinucleotide (10) because the expression and activity of the enzymatic machinery required for this conversion are markedly low (11–14). Niacin has been identified as a high-affinity ligand for the Gi-linked heterotrimeric guanine nucleotide-binding protein–coupled receptor (GPCR) hydroxycarboxylic acid receptor 2 (HCAR2), also known as GPR109A (15–17), which is expressed in the brain and has been shown to modulate microglial actions in several central nervous system (CNS) disease models (18–22). Specifically, HCAR2 activation with niacin and other ligands inhibits lipopolysaccharide–triggered inflammatory responses in microglial cells (18–20). Furthermore, niacin acts broadly through HCAR2 to elicit therapeutic effects in a demyelination model by improving microglial surveillance and increasing phagocytosis and cytokine production (21). Similarly, niacin treatment was beneficial in a glioblastoma model by increasing microglia chemotaxis and cytokine production (22). However, it is unknown whether HCAR2 modulation can

affect microglial functions in AD. We hypothesized that HCAR2 promotes a beneficial microglia phenotype in AD that can be pharmacologically stimulated by niacin.

Here, we report a robust induction of HCAR2 in the brain of the amyloidogenic 5xFAD mouse model and in patients with AD. Genetic inactivation of *Hcar2* in the 5xFAD mice impairs the microglial response to amyloid pathology, accompanied by an exacerbation of plaque burden, neuronal pathology, and ultimately, cognitive impairment. Conversely, persistent activation of HCAR2 with a U.S. Food and Drug Administration (FDA)–approved formulation of niacin, Niaspan, stimulates a broad and complex protective response mediated by microglia, leading to decreased plaque burden, reduced neuronal loss, and improved working memory deficits. Our findings support HCAR2 activation as a promising therapeutic strategy for AD.

RESULTS

Induction of HCAR2 by microglia in AD

To examine whether the expression of the GPCR HCAR2 is altered in AD, we analyzed *Hcar2* mRNA expression in the 5xFAD amyloidogenic mouse model and in human AD brain tissue (Fig. 1). *Hcar2* expression was increased in the hippocampus and cortex of 5xFAD animals during a period of active plaque deposition between 4 and 6 months of age in both females and males (Fig. 1A). To determine whether the expression of *Hcar2* is specifically associated with microglia, we depleted these cells in 4-month-old 5xFAD mice using the CSF1R antagonist PLX5622 (23). The depletion of about 70% of cortical microglia (24) reduced *Hcar2* mRNA expression in the 5xFAD brain (Fig. 1B, left). Furthermore, withdrawal of the CSF1R antagonist ($PLX^{on\text{-}off}$) resulted in the repopulation of microglia and the restoration of *Hcar2* expression (Fig. 1B, right). These results demonstrate that the induction of *Hcar2* expression in the 5xFAD brain is specifically associated with microglia. Because microgliosis could be the underlying reason for the increase in *Hcar2* mRNA expression, we analyzed a transcriptomic dataset of sorted microglia from 8.5-month-old 5xFAD mice (25, 26) and found that *Hcar2* expression increased within microglia cells in the 5xFAD brain (Fig. 1C, top). Moreover, incubation of primary murine microglia with 5 μM of $A\beta_{1\text{-}42}$ aggregates for 24 hours resulted in a significant increase ($P < 0.001$) in *Hcar2* expression (Fig. 1C, bottom), consistent with previous findings (27). To visualize the induction of *Hcar2* in the 5xFAD brain, we crossed 5xFAD mice with mice expressing a monomeric red fluorescent protein reporter (mRFP) under the endogenous murine *Hcar2* (5xFAD;$Hcar2^{mRFP}$), which has been previously reported to accurately reflect *Hcar2* expression (28, 29) and used to study *Hcar2* expression in microglia (30). Immunohistochemistry (IHC) of4-month-old B6 and 5xFAD;$Hcar2^{mRFP}$ animals revealed that *Hcar2* expression is restricted to ionized calcium binding adaptor molecule 1 (Iba1)-positive microglia (Fig. 1D), and it is markedly increased in cells surrounding Aβ plaques compared to adjacent uninvolved microglia (fig. S1A). Both mRFP and Iba1 colocalize with the microglia-specific marker P2RY12 (fig. S1B), validating that *Hcar2* is induced by brain-resident microglia in the 5xFAD brain, consistent with previous studies showing the lack of peripheral monocyte infiltration into the brain parenchyma of this model (31, 32). We also observed an induction of *Hcar2* mRNA in the brains of 4-month-old APPPS1

amyloidogenic mouse model (fig. S1C). Furthermore, published transcriptomic analysis of sorted microglia from the APPPS1 model (33) revealed that *Hcar2* mRNA was selectively increased in microglia associated with neuritic Aβ plaques [C-type lectin domain containing 7a (Clec7a)$^+$] compared with microglia not associated with Aβ plaques (Clec7a$^-$; fig. S1D), which is in accordance with our results in the 5xFAD model. Analysis of transcriptomic datasets revealed that *Hcar2* expression increases in microglia of PS19 tauopathy mice (fig. S1E) (34, 35), suggesting that tau pathology can also induce HCAR2 in AD.

We analyzed a human transcriptomic dataset of dorsolateral prefrontal cortex (BA9) tissue of 157 nondemented controls and 310 patients with AD (GSE33000) (36), which revealed increased *HCAR2* expression in AD (Fig. 1E). We validated this finding by analyzing *HCAR2* expression in postmortem brain tissue samples of control subjects and patients with AD by real-time quantitative polymerase chain reaction (qPCR; Fig. 1E). IHC of nondemented control (CTRL) and AD postmortem brain sections revealed that HCAR2 protein expression is selective for Iba1-positive cells and significantly increases ($P < 0.05$) in AD (Fig. 1F), which is consistent with our findings in the 5xFAD model (Fig. 1D). However, the induction of HCAR2 in the human AD brain does not seem limited to the immediate surroundings of amyloid plaques (Fig. 1F), as observed in the amyloid mouse models (Fig. 1D and fig. S1B), likely because of the robust and widespread presence of other triggers such as tau (fig. S1C), but it also might arise from nonspecific interactions of the antibody. Given the nonspecific immunoreactivity of many GPCR antibodies, we evaluated the specificity of the anti-HCAR2 antibody by small interfering RNA–mediated knockdown of HCAR2 in the human microglial cell line HMC3, which resulted in a corresponding reduction of HCAR2 immunoreactivity (fig. S1E). Overall, these findings support that HCAR2 is selectively expressed by microglia in the brain, which is consistent with RNA sequencing (RNA-seq) datasets (37, 38) and the previous identification of the *HCAR2* gene as part of a core human microglial signature (39). Furthermore, these data suggest an induction of HCAR2 in the AD brain.

Lack of *Hcar2* disrupts microglial actions in the amyloidogenic 5xFAD brain

Amyloid deposition starts very early in AD progression, decades before symptom onset (40) and initiates a microglial response that includes an increase in HCAR2 expression (Fig. 1). Thus, we sought to examine the role of HCAR2 in amyloid pathology by its genetic inactivation in the 5xFAD amyloidogenic model. We crossed 5xFAD with *Hcar2*$^{-/-}$ animals to obtain 5xFAD mice lacking the *Hcar2* gene (5xFAD;*Hcar2*$^{-/-}$). Lack of *Hcar2* was validated in brain tissue and primary microglia cultures of *Hcar2*$^{-/-}$ animals (fig. S2A). RNA from hippocampal tissue of 6-month-old female 5xFAD;*Hcar2*$^{+/+}$ and 5xFAD;*Hcar2*$^{-/-}$ mice was analyzed using the nCounter Glial Profiling Panel from NanoString, which comprises 770 genes mainly involved in glial cell biology and in neurotransmission. Differentially expressed genes (DEGs) [adjusted (adj.) $P < 0.05$] are shown in a heatmap (Fig. 2A). Inactivation of *Hcar2* lead to a significant down-regulation of 40 genes (adj. $P < 0.05$), and no genes were found to be significantly up-regulated (adj. $P > 0.05$). The Glial Profiling Panel contains genes that are expressed in microglia, astrocytes, oligodendrocytes, and neurons. However, more than half of the genes down-regulated by inactivation of *Hcar2* are selectively expressed in microglia compared to other cell types, as

documented in the Barres RNA-seq dataset (Fig. 2A) (37, 38), which is consistent with the specificity of HCAR2 for microglial cells in the brain (Fig. 1). Furthermore, enrichment analysis of Gene Ontology terms for Biological Process (GO BP) and WikiPathways indicates that lack of *Hcar2* represses pathways related to immune activation and response, prominently phagocytosis and the transmembrane immune signaling adaptor TYROBP pathway (Fig. 2B). Furthermore, GO Cellular Component enrichment analysis indicates that there is a decrease in the expression of cell surface and membrane components, which is consistent with reduced immune response and phagocytosis (Fig. 2B). The reduction of synaptic components in the absence of *Hcar2* also suggests an effect on neuronal function (Fig. 2B). We validated the reduction of several DEGs involved in microglia response and phagocytosis (*Spp1, Cst7, Cd68, Trem2, Tyrobp*, and *Axl*) by qPCR in 5xFAD;$Hcar2^{+/+}$ and 5xFAD;$Hcar2^{-/-}$. We also analyzed their expression in nontransgenic B6;$Hcar2^{+/+}$ and B6;$Hcar2^{-/-}$ (Fig. 2C). As expected, these genes were robustly increased in 5xFAD mice, compared to B6 controls; however, this induction was dampened (*Cst7, Cd68, Trem2*, and *Tyrobp*) or even abolished (*Spp1* and *Axl*) by *Hcar2* inactivation (Fig. 2C). We observed no changes in gene expression between B6;$Hcar2^{+/+}$ and B6;$Hcar2^{-/-}$ by qPCR, indicating that *Hcar2* does not affect these pathways in the nondiseased brain. Overall, these data suggest that lack of *Hcar2* leads to a deficient response by microglia to amyloid pathology, prominently associated with decreased phagocytosis and TYROBP signaling.

Lack of *Hcar2* curtails microglia engagement with plaques and increases plaque burden

We proceeded with further functional and phenotypic analysis of 5xFAD;$Hcar2^{+/+}$ and 5xFAD:$Hcar2^{-/-}$ mice to understand how the observed transcriptional differences (Fig. 2) effectively translate into alterations of the microglial response and severity of amyloid pathology. Thus, we investigated the impact of *Hcar2* on plaque pathology and microglia-plaque interactions in the 5xFAD brain. The subiculum region exhibits the earliest and most aggressive amyloid accumulation in the 5xFAD model (41). We observed a significant increase ($P < 0.05$) in the number of thioflavin S–positive plaques and the area occupied by these plaques in the subiculum of 4- and 6-month-old 5xFAD mice lacking *Hcar2* of both sexes (Fig. 3A and fig. S3, A and B). Plaque burden was modestly increased in the hippocampus (excluding subiculum) of 4-month-old animals (fig. S3C) and in the cortex of 6-month-old female 5xFAD mice lacking *Hcar2* (fig. S3A), which is accompanied by an increase in astrocytosis (fig. S3D). The increased plaque burden in the subiculum of 4-month-old 5xFAD;$Hcar2^{-/-}$ mice is accompanied by reduced Iba1 percent area (Fig. 3B). In agreement, inactivation of *Hcar2* leads to reduced *Aif1* expression in the hippocampus of 4-month-old 5xFAD but not in nontransgenic control (B6) mice (Fig. 3B), indicating that this effect is not present in a nondiseased brain. We further examined microglia response to amyloid pathology by IHC at a later stage of disease in 6-month-old 5xFAD mice. Similar to 4-month-old animals, lack of *Hcar2* reduces Iba1 percent area in the subiculum (Fig. 3C), accompanied by a decrease in microglial envelopment of plaques (Fig. 3C). A similar reduction was observed in the cortex of 5xFAD;$Hcar2^{-/-}$ mice (Fig. 3D). We quantified microglia abundance within a radius of 25 μm around each plaque to assess microglia recruitment to plaques, which was significantly reduced ($P < 0.001$) in the absence of *Hcar2* (Fig. 3E). Overall, these data support that lack of *Hcar2* leads to a deficient microglia coverage and engagement with plaques, which is associated with higher plaque burden.

Hcar2 is required for efficient microglia proliferation and amyloid uptake

We observed an inhibition of the microglial response in 5xFAD;*Hcar2*$^{-/-}$ mice, which results in aggravated plaque burden. Because the area occupied by microglia is decreased in the brains of 5xFAD; *Hcar2*$^{-/-}$ compared to 5xFAD;*Hcar2*$^{+/+}$ mice, we hypothesized that HCAR2 regulates proliferation of microglia in response to amyloid pathology. We analyzed whether the absence of *Hcar2* affects the expression of the proliferation marker Ki-67 in the brains of 4-month-old 5xFAD animals. By IHC, we observed significantly fewer ($P < 0.05$) Ki-67–positive microglia (Ki-67^{+}/Iba1^{+}) in the brains of 5xFAD mice lacking *Hcar2* (Fig. 4A), indicating reduced proliferation. Ki-67 staining was observed exclusively within cell nuclei (fig. S4A). Because microglial proliferative capacity has been correlated with increased phagocytic activity (42–44), this reduction in proliferation, together with the reduced expression of phagocytic genes (Fig. 2) and increased plaque burden (Fig. 3) observed in 5xFAD;*Hcar2*$^{-/-}$, suggests that the lack of *Hcar2* leads to defects in Aβ phagocytosis. Thus, we examined how HCAR2 affects total number of microglia and amyloid uptake in the 5xFAD brain by flow cytometry. We performed an in vivo microglia phagocytosis assay by intraperitoneal administration of methoxy-X04 (Aβ marker) in 6-month-old 5xFAD;*Hcar2*$^{-/-}$ and 5xFAD;*Hcar2*$^{+/+}$ animals 3 hours before proceeding to flow cytometry as previously described (45). Microglia were identified by gating for CD11b^{+} cells (fig. S4B), and in agreement with reduced microglia coverage and proliferation, we observed a significant reduction ($P < 0.05$) in the number of microglia cells in 5xFAD;*Hcar2*$^{-/-}$ compared to 5xFAD;*Hcar2*$^{+/+}$ animals (Fig. 4B). On the basis of the expression of CD45, microglia can be stratified into CD45^{low} (less activated) and CD45^{int} (more activated) (fig. S4C). *Hcar2* inactivation significantly reduced ($P < 0.05$) the number of cells solely in the CD45^{int} population, with no significant effects ($P = 0.09$) on CD45^{low} cells (Fig. 4C). Thus, as expected, the absence of *Hcar2* reduced the proportion of CD45^{int} cells within the total microglia population (CD11b^{+}) while increasing the proportion of CD45^{low} cells, suggesting that lack of *Hcar2* limits the activation of microglia triggered by amyloid pathology (Fig. 4C). The decrease in microglial numbers (CD11b^{+} cells) was also accompanied by a robust overall reduction of Aβ uptake (methoxy-X04^{+}) by this population in 5xFAD;*Hcar2*$^{-/-}$ animals (Fig. 4D). The percentage of CD11b^{+} cells positive for methoxy-X04 was only mildly reduced in *Hcar2* knockout animals (fig. S4C), suggesting that HCAR2 exerts a minor effect on the intrinsic capacity of microglia to take up Aβ. However, this analysis might not accurately reflect the entire magnitude of HCAR2 effects on Aβ uptake. The percentage of cells phagocytosing Aβ might be inflated in 5xFAD;*Hcar2*$^{-/-}$ animals purely because these mice rely on fewer microglia to clear more Aβ, which can obscure deficits in their inherent capacity to uptake amyloid. Thus, to further examine whether HCAR2 affects the intrinsic ability of microglia to uptake Aβ, we cultured primary murine microglia from *Hcar2*$^{+/+}$ and *Hcar2*$^{-/-}$ mice and incubated the cells with an FDA-approved formulation of niacin (Niaspan) at 1 mM for 24 hours to activate HCAR2, followed by incubation with 1.25 μM of HiLyte Fluor 488–labeled $A\beta_{1-42}$ aggregates for 30 min. Our results show that the basal uptake of $A\beta_{1-42}$ was decreased in *Hcar2*$^{-/-}$ microglia (Fig. 4E). Moreover, Niaspan treatment increased $A\beta_{1-42}$ uptake in *Hcar2*$^{+/+}$ cells but not in *Hcar2*$^{-/-}$ microglia (Fig. 4E), validating that niacin acted through HCAR2 to increase Aβ uptake. Furthermore, treatment of *Hcar2*$^{+/+}$ microglia with lower concentrations of niacin (100 μM) led to a significant increase ($P < 0.05$) in the uptake of Aβ as well, which was

not observed in *Hcar2*$^{-/-}$ cells (fig. S4E). These results are consistent with previous findings showing that HCAR2 stimulates phagocytosis of beads and myelin debris by microglia (20, 21). In summary, these data demonstrate that HCAR2 is required for efficient microglia proliferation and Aβ uptake in the context of amyloid pathology.

Lack of *Hcar2* exacerbates amyloid-associated neuropathology

Our transcriptomic analyses suggest a disruption of neuronal function in 5xFAD;*Hcar2*$^{-/-}$ compared to 5xFAD;*Hcar2*$^{+/+}$ mice (Fig. 2B). We evaluated working memory in B6 and 5xFAD mice (*Hcar2*$^{+/+}$ and *Hcar2*$^{-/-}$) using the Y-maze task. This assay has been widely used in the 5xFAD model, which shows a robust deficit in working memory starting at around 4 to 5 months of age (41). We analyzed 4-month-old mice, and although working memory impairments are still not evident in 5xFAD;*Hcar2*$^{+/+}$ animals at this age, 5xFAD mice lacking *Hcar2* already exhibited significant deficits ($P < 0.05$), which was not associated with the number of arm entries (Fig. 5A). Both female and male mice were analyzed together because we observed no sex-dependent differences within each genotype at this age. We also assessed motor skills (speed and distance) and anxiety-like behavior (time immobile) during the Y-maze task between all genotypes and found no significant differences ($P > 0.05$; fig. S5A).

In the 5xFAD model, the subiculum undergoes severe neuronal loss as disease progresses. IHC analysis of NeuN-positive cells revealed increased neuronal loss in the subiculum of 4-month-old 5xFAD;*Hcar2*$^{-/-}$ compared to 5xFAD;*Hcar2*$^{+/+}$ mice (Fig. 5B). Dystrophic neurites (DNs) are swollen abnormal neurites, abundant in the vicinity of Aβ deposits within the brains of patients with AD and 5xFAD mice (46, 47). DNs are enriched in lysosomal-associated membrane protein 1 (LAMP-1) and ubiquitin and accumulate neuronal N-terminal APP (N-APP) (48, 49). IHC analysis revealed an increased colocalization of LAMP-1 and ubiquitin with N-APP within the subiculum of 5xFAD;*Hcar2*$^{-/-}$ (Fig. 5C), although the percent area of LAMP-1 and ubiquitin remained similar between 5xFAD;*Hcar2*$^{+/+}$ and 5xFAD;*Hcar2*$^{-/-}$ animals (fig. S5B). In agreement, analysis of N-APP staining within individual DNs revealed increased accumulation of N-APP in 5xFAD;*Hcar2*$^{-/-}$ mice (Fig. 5C). We found a significant correlation ($P < 0.05$) between higher content of N-APP in DNs and reduced neuronal numbers (fig. S5C). These results demonstrate that inactivation of *Hcar2* exacerbates neuronal pathology in 5xFAD, including increased neuronal loss that was associated with accelerated onset of working memory deficits.

Pharmacological activation of HCAR2 with Niaspan reduces amyloid pathology in 5xFAD mice

To determine whether the pharmacological activation of HCAR2 could stimulate a beneficial microglial response after onset of amyloid pathology, we treated 5xFAD animals with the FDA-approved oral formulation of niacin, Niaspan. It is well documented that female 5xFAD mice exhibit a more aggressive amyloid pathology compared to males (50). Because both 5xFAD males and females revealed similar increase in *Hcar2* expression and similar exacerbation of amyloid pathology associated with the lack of *Hcar2* (Figs. 1, 3, and 5), we opted to eliminate sex-dependent confounds by analyzing the effects of HCAR2

activation only in male mice. To mimic treatment in a symptomatic stage of disease, we started Niaspan administration in 5-month-old 5xFAD animals, which already exhibited working memory deficits (fig. S6A). Animals were treated with Niaspan (100 mg/kg) for 30 days by oral gavage. This dose resulted in a significant increase ($P < 0.001$) of niacin concentration in 5xFAD brain (≈6-fold) 30 min after administration (fig. S6B). Treatment of 5xFAD mice with Niaspan rescued working memory deficits (Fig. 6A), demonstrating a robust therapeutic effect of niacin. As expected, Niaspan did not alter working memory in B6 mice (Fig. 6A). The behavioral improvement in 5xFAD mice treated with Niaspan was accompanied by reduced neuronal loss in the subiculum analyzed by NeuN staining (Fig. 6B). Imaging of thioflavin S–positive plaques revealed that treatment of Niaspan reduced plaque number and area, most prominently, not only in the subiculum but also in the hippocampus and cortex. (Fig. 6B and fig. S6C). Furthermore, plaque size was reduced in the subiculum of treated animals (fig. S6D). We have also observed by IHC that Iba1 is entirely colocalized with the microglia-specific marker P2RY12 in Niaspan-treated animals, supporting that this treatment does not induce infiltration of peripheral-derived monocytes into the brain parenchyma of 5xFAD (fig. S6E). These data demonstrate that Niaspan is able to reduce plaque burden and neuronal pathology in the 5xFAD mice. Because the subiculum was shown to be the most sensitive area to Niaspan treatment, we analyzed the microglial response in this region. Reduced plaque burden is accompanied by a mild decrease of Iba1 percent area in Niaspan-treated animals, although plaque coverage by microglia remains similar between vehicle and treated animals (Fig. 6D). Because both plaque and Iba1 areas decrease with Niaspan treatment, to compare microglia response to amyloid deposition between untreated and treated animals, we determined the ratio of microglia area to plaque area. The ratio of Iba1 area/thioflavin S area was increased in Niaspan-treated mice (Fig. 6E), which indicates that Niaspan induced a more efficient mobilization of microglia in response to Aβ deposition. Furthermore, genes related to plaque engagement and amyloid uptake down-regulated in 5xFAD;*Hcar2*$^{-/-}$ mice (Fig. 2) were found to be increased in the hippocampus of Niaspan-treated mice (*Trem2, Axl*, and *Cd68*) (Fig. 6F). We added *Mrc1* to the qPCR analysis because this microglial gene involved in phagocytosis has been shown to be regulated by HCAR2 (20) and is not included in the nCounter Glial Profiling Panel. *Mrc1* increases with Niaspan treatment (Fig. 6F). Furthermore, *Clec7a* is an important marker of microglia engagement with plaques in AD (33), and we observed a significant induction ($P < 0.01$) of its expression by Niaspan treatment (Fig. 6F), whereas NanoString analysis of *Hcar2*$^{-/-}$ mice revealed no effects on *Clec7a* expression (fold change = 0.749, $P = 0.032$, adj. $P = 0.143$). Although plaque envelopment is similar between untreated and treated animals, the induction of genes related to plaque engagement and amyloid uptake by Niaspan suggests increased efficiency of microglia in reducing amyloid deposition, which is supported by our in vitro phagocytosis assay (Fig. 4E). Furthermore, using a Meso Scale Discovery (MSD) cytokine panel, we observed that microglia stimulation by Niaspan does not elicit overall changes in brain cytokine concentration, except for a mild increase interferon-γ (IFN-γ) (Fig. 6G), which has been reported to have potential beneficial effects in AD (51, 52).

To validate that Niaspan exerts its beneficial effects through HCAR2, we evaluated the same dosage paradigm using 5xFAD;*Hcar2*$^{-/-}$ mice. In the absence of *Hcar2*, we did not observe

an improvement in working memory nor a reduction in neuronal loss in 5xFAD mice treated with Niaspan (Fig. 7, A and B). In addition, neither plaque burden nor microglia coverage were altered with Niaspan treatment in the 5xFAD;*Hcar2*$^{-/-}$ mice (Fig. 7, C and D). The Niaspan-mediated induction of genes related to plaque envelopment and amyloid uptake and the increase of IFN-γ observed in 5xFAD;*Hcar2*$^{+/+}$ were abolished in the absence of *Hcar2* (Fig. 7, E and F). These observations demonstrate that Niaspan acts through HCAR2 to stimulate a beneficial microglia response and attenuate amyloid pathology, which validates the targeting of this receptor as a potential therapeutic strategy for AD.

DISCUSSION

Microglia have emerged as a crucial player in AD pathogenesis and progression (2–4). The characterization and systematization of microglia transcriptional signatures in AD and other CNS disorders have led to a more nuanced understanding of the multifaceted roles of these cells in the normal and diseased brain (33, 53, 54). Microglia represent a highly plastic and heterogenous population that can exhibit a plethora of phenotypes in AD, which confounds the development of effective therapeutic strategies directed at these cells. Thus, the study of specific microglial phenotypes remains critical to understand how to modulate microglia to achieve therapeutic effects in AD. Here, we report that the niacin receptor, HCAR2, acts to limit disease progression in the amyloidogenic mouse model 5xFAD by stimulating a protective response of microglia to amyloid pathology. HCAR2 is required for efficient microglia proliferation, engagement with amyloid deposits, and engulfment of Aβ, which are important microglial features commonly implicated in microglia phenotypes reported to be beneficial in AD (55–59). The present study reports a therapeutic strategy for AD tailored to potentiate microglia neuroprotective actions through the stimulation of HCAR2. The pharmacological activation of HCAR2 could be achieved by an FDA-approved formulation of niacin, Niaspan, with relatively minor adverse side effects (60), which might be repurposed for AD in the clinical setting.

The strategy to pharmacologically stimulate HCAR2 in AD takes advantage that the expression of this receptor is robustly induced by microglia in the AD brain, which sensitizes these cells to the actions of HCAR2 ligands. The increase in HCAR2 expression is robustly induced by amyloid deposition that starts very early in AD progression, and to a lesser extent, by tau pathology that is present at later stages of AD progression and other tauopathies.

Niaspan treatment leads to a broad range of positive effects in 5xFAD animals, including reduction of plaque burden and neuronal loss, as well as rescue of working memory deficits. The biological actions of niacin are not limited to HCAR2 activation (10); however, our data show that the beneficial effects of Niaspan in the 5xFAD brain are dependent on the presence of *Hcar2*. The dose of Niaspan (100 mg/kg) selected to treat 5xFAD mice was determined on the basis of available literature (61–63). Furthermore, according to the human equivalent doses based on body surface area (64), the dosage of Niaspan used to treat mice corresponds to a daily dosage of about 500 mg of Niaspan in humans, which is well below the daily maintenance dose used to treat dyslipidemia (1000 to 2000 mg). Thus, our findings suggest that a low and safe dose of Niaspan might be sufficient to elicit

therapeutic effects in AD and are consistent with the existing epidemiological data showing that enhanced dietary niacin is associated with reduced risk for AD (6). Nonetheless, oral administration of niacin often results in cutaneous flushing, which is triggered by HCAR2-mediated production of prostaglandins D2 and E2 by COX-1 and COX-2 within epidermal Langerhans cells and keratinocytes (29, 65). This side effect can be attenuated by aspirin or other COX inhibitors or by antagonism of prostaglandin receptors such as DP1 (29, 65, 66). Niaspan treatment rapidly and robustly increases niacin concentration in the brain of 5xFAD mice, validating niacin ability to cross the blood-brain barrier and exert direct effects in the brain, namely, on microglia. Although we only used male 5xFAD mice in our treatment cohort with Niaspan, our data clearly support an identical role of HCAR2 in amyloid pathology between sexes. Niaspan treatment of 5xFAD animals was initiated after the onset of robust amyloid pathology. The animals were treated at 5 months, a stage of disease in which cognitive deficits are already present because of widespread amyloid deposition and associated neuropathology. These data support that niacin could potentially be administered after onset of robust amyloid pathology and perhaps even in symptomatic stages of AD. Nonetheless, further studies are necessary to assess the efficacy of Niaspan after longer periods of treatment and its effects on different pathological aspects of AD, namely, tau pathology.

The stimulation of microglial response through HCAR2 described in this work is consistent with two recent studies using different models of CNS disease. In each of these cases, niacin treatment induced a broad response from myeloid cells that attenuated pathogenic effects. One study reported that niacin is beneficial in a model of demyelination by modulating macrophages/microglia through HCAR2, underlined by increased microglia coverage, cytokine production, and phagocytosis efficiency (21). Another study using a murine brain tumor model also reported that niacin functioned as immune stimulator and reactivated inefficient macrophages/microglia to control tumor growth (22). Both studies report a stimulatory effect of niacin on the myeloid population present in diseased CNS, composed of both peripherally derived macrophages and microglia. These findings suggest that the effects of Niaspan on microglia documented in this study might be extendable to peripherally derived macrophages that may be present in the human AD brain. Furthermore, niacin has also been investigated as a therapeutic agent for Parkinson’s disease because of its immunomodulatory and neuroprotective properties (18, 67, 68). Clinical trials of niacin for Parkinson’s disease and glioblastoma are currently in progress (NCT03808961 and NCT04677049, respectively). The ability of HCAR2 to modulate the functions of microglia and other immune cells in different contexts suggests a broader role for this receptor in CNS diseases with a neuroimmune component.

There are some limitations to this study. Although our results indicate that microglial HCAR2 acts directly to modulate amyloid pathology, a cautious interpretation is warranted because our in vivo analysis focused on a constitutive knockout of *Hcar2* and systemic delivery of Niaspan. Although it has been shown that 5xFAD mice do not exhibit infiltration of peripheral monocytes into the brain (31, 32), we cannot rule out that peripheral cells expressing HCAR2 may also indirectly contribute to the modulation of microglia and amyloid pathology, for example, through soluble factors. The analysis of a murine model with inducible microglia-specific inactivation of *Hcar2* will be an important extension of

this study, as well as the identification of the molecular mechanisms underlying HCAR2 actions on microglia in AD. We report that 5xFAD mice lacking *Hcar2* exhibited a deficient microglia response, which includes a reduction of a subset of transcripts involved in phagocytosis and immune response. However, we did not assess whether the lack of *Hcar2* leads to decreased expression and signaling of these genes by direct regulation or is due to the observed reduction in microglia numbers or both, which will be important to analyze in future studies. Although several reports have explored HCAR2 signaling pathways in different cell types linked to its roles in regulating lipid metabolism and immune functions (20, 69–73), the microglial pathways directly regulated by HCAR2 in AD remain largely unexplored.

In summary, we report a therapeutic strategy to modulate microglia functions in AD through the niacin receptor HCAR2, which is required for an efficient microglia response to pathology. We demonstrate that HCAR2 activation with an FDA-approved formulation of niacin, Niaspan, leads to reduced plaque burden and neuronal pathology and rescue of working memory deficits in the 5xFAD mouse model. Thus, niacin is a promising therapeutic agent for AD with a high translational potential for clinical use.

MATERIALS AND METHODS

Study design

The aim of this study was to determine the therapeutic potential of niacin receptor HCAR2 in AD. We first analyzed the role of HCAR2 in the progression of amyloid pathology in the AD mouse model 5xFAD. Once we concluded that HCAR2 was responsible for protective microglial phenotype in the 5xFAD brain, we tested the hypothesis that pharmacological activation of HCAR2 with the FDA-approved niacin formulation Niaspan could elicit therapeutic effects in the 5xFAD model. Mice were randomly divided into vehicle or Niaspan groups. Sample sizes were selected on the basis of pilot experiments and previous extensive experience with the 5xFAD model and microglia cultures (24, 74–76). For biochemical outcomes, we used a minimum n of three mice in each experimental group/genotype, mostly $n \geq 4$. For behavioral outcomes, we used a minimum of six mice per group/genotype. Y-maze and IHC analysis were performed by investigators blinded to genotype/treatment. Gene expression and flow cytometry analysis were performed unblinded. All animal studies have been approved by the Indiana University School of Medicine Institutional American Association for Laboratory Animal Science Care and Use Committee.

Animal models

5xFAD mice was obtained from the Jackson Laboratory (stock no. 34840-JAX) and expresses five human familial AD mutations driven by the mouse Thy1 promoter (APPSwFlLon, PSEN1*M146L* L286V]6799Vas) (41). The APPPS1-21 mouse model (provided by M. Jucker) expresses the Swedish APP mutation (KM670/671NL) and the L166P mutation in PSEN1 driven under the Thy1 promoter (77). C57BL/6 *Hcar2*$^{-/-}$ animals (15) were provided by V. Ganapathy and S. Offermanns and crossed to 5xFAD animals.

C57BL/6 *Hcar2*^{mRFP} mice (28, 29) were provided by M. Schwaninger and S. Offermanns. Four- and 6-month-old male and female mice were used as detailed in Results.

Statistical analysis

Statistical analysis was performed using GraphPad Prism version 8 for Windows (GraphPad Software; www.graphpad.com). Data were first analyzed for normality followed by statistical tests. The tests used were Student's *t* test, Mann-Whitney test, one-way analysis of variance (ANOVA) test followed by Tukey's post hoc test, and Kruskal-Wallis test followed by Dunn's post hoc test. Two-way ANOVA test was also applied when it was required to analyze the effect of two independent variables (factors) on a dependent variable. If interaction between the factors (P^{int}) was found significant ($P < 0.05$) for a particular experiment, then the *P* values for the main effects are not reported. Two-way ANOVA was followed by Tukey's post hoc tests.

Supplementary Material

Refer to Web version on PubMed Central for supplementary material.

Acknowledgments:

The *Hcar2*$^{-/-}$ and *Hcar2*^{mRFP} mouse models (15, 28, 29) were a gift from S. Offermanns (Max Planck Institute for Heart and Lung Research, Germany) and provided by V. Ganapathy (Texas Tech University, Health Sciences Center, USA) and M. Schwaninger (Institute for Experimental and Clinical Pharmacology and Toxicology, University of Lübeck, Lübeck, Germany). We thank A. Shekhar and J. Patel (Indiana University) for assistance with the behavioral assays. Nicotinic acid quantification was provided by the Clinical Pharmacology Analytical Core (CPAC) at Indiana University School of Medicine. AD and control tissues for this research were provided by J. C. Troncoso at the Johns Hopkins University Alzheimer Disease Research Center (NIA P50 AG05146). Graphical abstract was created with BioRender.com.

Funding:

This work was supported by grants from the NIH, RF1 AG051495 (B.T.L. and G.E.L.) and RF1 AG050597203 (G.E.L.), the Indiana CTSI Eli Lilly-Stark Neurosciences Post-Doctoral Research Fellowship in Neurodegeneration (M.M.), the Alzheimer's Association Research Fellowship 2019-AARF-643631 (M.M.), and the IU Simon Comprehensive Cancer Center Support Grant P30 CA082709 (CPAC).

Data and materials availability:

All data associated with this study are present in the paper or the Supplementary Materials. Expression data obtained from external Gene Expression Omnibus (GEO) datasets and publications have been referenced in the text and/or figures. Requests for resources or reagents should be directed to G.E.L.

REFERENCES AND NOTES

1. Selkoe DJ, Hardy J, The amyloid hypothesis of Alzheimer's disease at 25 years. EMBO Mol. Med 8, 595–608 (2016). [PubMed: 27025652]
2. Hansen DV, Hanson JE, Sheng M, Microglia in Alzheimer's disease. J. Cell Biol 217, 459–472 (2018). [PubMed: 29196460]
3. Karch CM, Goate AM, Alzheimer's disease risk genes and mechanisms of disease pathogenesis. Biol. Psychiatry 77, 43–51 (2015). [PubMed: 24951455]

4. Sims R, van der Lee SJ, Naj AC, Bellenguez C, Badarinarayan N, Jakobsdottir J, Kunkle BW, Boland A, Raybould R, Bis JC, Martin ER, Grenier-Boley B, Heilmann-Heimbach S, Chouraki V, Kuzma AB, Sleegers K, Vronskaya M, Ruiz A, Graham RR, Olaso R, Hoffmann P, Grove ML, Vardarajan BN, Hiltunen M, Nothen MM, White CC, Hamilton-Nelson KL, Epelbaum J, Maier W, Choi SH, Beecham GW, Dulary C, Herms S, Smith AV, Funk CC, Derbois C, Forstner AJ, Ahmad S, Li H, Bacq D, Harold D, Satizabal CL, Valladares O, Squassina A, Thomas R, Brody JA, Qu L, Sanchez-Juan P, Morgan T, Wolters FJ, Zhao Y, Garcia FS, Denning N, Fornage M, Malamon J, Naranjo MCD, Majounie E, Mosley TH, Dombroski B, Wallon D, Lupton MK, Dupuis J, Whitehead P, Fratiglioni L, Medway C, Jian X, Mukherjee S, Keller L, Brown K, Lin H, Cantwell LB, Panza F, McGuinness B, Moreno-Grau S, Burgess JD, Solfrizzi V, Proitsi P, Adams HH, Allen M, Seripa D, Pastor P, Cupples LA, Price ND, Hannequin D, Frank-Garcia A, Levy D, Chakrabarty P, Caffarra P, Giegling I, Beiser AS, Giedraitis V, Hampel H, Garcia ME, Wang X, Lannfelt L, Mecocci P, Eiriksdottir G, Crane PK, Pasquier F, Boccardi V, Henandez I, Barber RC, Scherer M, Tarraga L, Adams PM, Leber M, Chen Y, Albert MS, Riedel-Heller S, Emilsson V, Beekly D, Braae A, Schmidt R, Blacker D, Masullo C, Schmidt H, Doody RS, Spalletta G, Longstreth WT Jr., Fairchild TJ, Bossu P, Lopez OL, Frosch MP, Sacchinelli E, Ghetti B, Yang Q, Huebinger RM, Jessen F, Li S, Kamboh MI, Morris J, Sotolongo-Grau O, Katz MJ, Corcoran C, Dunstan M, Braddel A, Thomas C, Meggy A, Marshall R, Gerrish A, Chapman J, Aguilar M, Taylor S, Hill M, Fairen MD, Hodges A, Vellas B, Soininen H, Kloszewska I, Daniilidou M, Uphill J, Patel Y, Hughes JT, Lord J, Turton J, Hartmann AM, Cecchetti R, Fenoglio C, Serpente M, Arcaro M, Caltagirone C, Orfei MD, Ciaramella A, Pichler S, Mayhaus M, Gu W, Lleo A, Fortea J, Blesa R, Barber IS, Brookes K, Cupidi C, Maletta RG, Carrell D, Sorbi S, Moebus S, Urbano M, Pilotto A, Kornhuber J, Bosco P, Todd S, Craig D, Johnston J, Gill M, Lawlor B, Lynch A, Fox NC, Hardy J, Consortium A, Albin RL, Apostolova LG, Arnold SE, Asthana S, Atwood CS, Baldwin CT, Barnes LL, Barral S, Beach TG, Becker JT, Bigio EH, Bird TD, Boeve BF, Bowen JD, Boxer A, Burke JR, Burns JM, Buxbaum JD, Cairns NJ, Cao C, Carlson CS, Carlsson CM, Carney RM, Carrasquillo MM, Carroll SL, Diaz CC, Chui HC, Clark DG, Cribbs DH, Crocco EA, DeCarli C, Dick M, Duara R, Evans DA, Faber KM, Fallon KB, Fardo DW, Farlow MR, Ferris S, Foroud TM, Galasko DR, Gearing M, Geschwind DH, Gilbert JR, Graff-Radford NR, Green RC, Growdon JH, Hamilton RL, Harrell LE, Honig LS, Huentelman MJ, Hulette CM, Hyman BT, Jarvik GP, Abner E, Jin LW, Jun G, Karydas A, Kaye JA, Kim R, Kowall NW, Kramer JH, LaFerla FM, Lah JJ, Leverenz JB, Levey AI, Li G, Lieberman AP, Lunetta KL, Lyketsos CG, Marson DC, Martiniuk F, Mash DC, Masliah E, McCormick WC, McCurry SM, McDavid AN, McKee AC, Mesulam M, Miller BL, Miller CA, Miller JW, Morris JC, Murrell JR, Myers AJ, O'Bryant S, Olichney JM, Pankratz VS, Parisi JE, Paulson HL, Perry W, Peskind E, Pierce A, Poon WW, Potter H, Quinn JF, Raj A, Raskind M, Reisberg B, Reitz C, Ringman JM, Roberson ED, Rogaeva E, Rosen HJ, Rosenberg RN, Sager MA, Saykin AJ, Schneider JA, Schneider LS, Seeley WW, Smith AG, Sonnen JA, Spina S, Stern RA, Swerdlow RH, Tanzi RE, Thornton-Wells TA, Trojanowski JQ, Troncoso JC, Van Deerlin VM, Van Eldik LJ, Vinters HV, Vonsattel JP, Weintraub S, Welsh-Bohmer KA, Wilhelmsen KC, Williamson J, Wingo TS, Woltjer RL, Wright CB, Yu CE, Yu L, Garzia F, Golamaully F, Septier G, Engelborghs S, Vandenberghe R, De Deyn PP, Fernadez CM, Benito YA, Thonberg H, Forsell C, Lilius L, Kinhult-Stahlbom A, Kilander L, Brundin R, Concari L, Helisalmi S, Koivisto AM, Haapasalo A, Dermecourt V, Fievet N, Hanon O, Dufouil C, Brice A, Ritchie K, Dubois B, Himali JJ, Keene CD, Tschanz J, Fitzpatrick AL, Kukull WA, Norton M, Aspelund T, Larson EB, Munger R, Rotter JI, Lipton RB, Bullido MJ, Hofman A, Montine TJ, Coto E, Boerwinkle E, Petersen RC, Alvarez V, Rivadeneira F, Reiman EM, Gallo M, O'Donnell CJ, Reisch JS, Bruni AC, Royall DR, Dichgans M, Sano M, Galimberti D, George-Hyslop PS, Scarpini E, Tsuang DW, Mancuso M, Bonuccelli U, Winslow AR, Daniele A, Wu CK, GERAD/PERADES, CHARGE, ADGC, EADI, Peters O, Nacmias B, Riemenschneider M, Heun R, Brayne C, Rubinsztein DC, Bras J, Guerreiro R, Al-Chalabi A, Shaw CE, Collinge J, Mann D, Tsolaki M, Clarimon J, Sussams R, Lovestone S, O'Donovan MC, Owen MJ, Behrens TW, Mead S, Goate AM, Uitterlinden AG, Holmes C, Cruchaga C, Ingelsson M, Bennett DA, Powell J, Golde TE, Graff C, De Jager PL, Morgan K, Ertekin-Taner N, Combarros O, Psaty BM, Passmore P, Younkin SG, Berr C, Gudnason V, Rujescu D, Dickson DW, Dartigues JF, DeStefano AL, Ortega-Cubero S, Hakonarson H, Campion D, Boada M, Kauwe JK, Farrer LA, Van Broeckhoven C, Ikram MA, Jones L, Haines JL, Tzourio C, Launer LJ, Escott-Price V, Mayeux R, Deleuze JF, Amin N, Holmans PA, Pericak-Vance MA, Amouyel P, van Duijn CM, Ramirez A, Wang LS, Lambert JC, Seshadri S, Williams J, Schellenberg GD, Rare

coding variants in PLCG2, ABI3, and TREM2 implicate microglial-mediated innate immunity in Alzheimer's disease. Nat. Genet 49, 1373–1384 (2017). [PubMed: 28714976]

5. Qin B, Xun P, Jacobs DR Jr, Zhu N, Daviglus ML, Reis JP, Steffen LM, Van Horn L, Sidney S, He K, Intake of niacin, folate, vitamin B-6, and vitamin B-12 through young adulthood and cognitive function in midlife: The Coronary Artery Risk Development in Young Adults (CARDIA) study. Am. J. Clin. Nutr 106, 1032–1040 (2017). [PubMed: 28768650]
6. Morris MC, Evans DA, Bienias JL, Scherr PA, Tangney CC, Hebert LE, Bennett DA, Wilson RS, Aggarwal N, Dietary niacin and the risk of incident Alzheimer's disease and of cognitive decline. J. Neurol. Neurosurg. Psychiatry 75, 1093–1099 (2004). [PubMed: 15258207]
7. Hankes LV, Coenen HH, Rota E, Langen KJ, Herzog H, Wutz W, Stoecklin G, Feinendegen LE, Effect of Huntington's and Alzheimer's diseases on the transport of nicotinic acid or nicotinamide across the human blood-brain barrier. Adv. Exp. Med. Biol 294, 675–678 (1991). [PubMed: 1837697]
8. Dastur DK, Santhadevi N, Quadros EV, Avari FC, Wadia NH, Desai MN, Bharucha EP, The B-vitamins in malnutrition with alcoholism: A model of intervitamin relationships. Br. J. Nutr 36, 143–159 (1976). [PubMed: 182198]
9. van der Velpen V, Rosenberg N, Maillard V, Teav T, Chatton JY, Gallart-Ayala H, Ivanisevic J, Sex-specific alterations in NAD+ metabolism in 3xTg Alzheimer's disease mouse brain assessed by quantitative targeted LC-MS. J. Neurochem 159, 378–388 (2021). [PubMed: 33829502]
10. Verdin E, NAD(+) in aging, metabolism, and neurodegeneration. Science 350, 1208–1213 (2015). [PubMed: 26785480]
11. Duarte-Pereira S, Pereira-Castro I, Silva SS, Correia MG, Neto C, da Costa LT, Amorim A, Silva RM, Extensive regulation of nicotinate phosphoribosyltransferase (NAPRT) expression in human tissues and tumors. Oncotarget 7, 1973–1983 (2016). [PubMed: 26675378]
12. Cole J, Guiot MC, Gravel M, Bernier C, Shore GC, Roulston A, Novel NAPRT specific antibody identifies small cell lung cancer and neuronal cancers as promising clinical indications for a NAMPT inhibitor/niacin co-administration strategy. Oncotarget 8, 77846–77859 (2017). [PubMed: 29100430]
13. Hara N, Yamada K, Shibata T, Osago H, Hashimoto T, Tsuchiya M, Elevation of cellular NAD levels by nicotinic acid and involvement of nicotinic acid phosphoribosyltransferase in human cells. J. Biol. Chem 282, 24574–24582 (2007). [PubMed: 17604275]
14. Zamporlini F, Ruggieri S, Mazzola F, Amici A, Orsomando G, Raffaelli N, Novel assay for simultaneous measurement of pyridine mononucleotides synthesizing activities allows dissection of the NAD(+) biosynthetic machinery in mammalian cells. FEBS J. 281, 5104–5119 (2014). [PubMed: 25223558]
15. Tunaru S, Kero J, Schaub A, Wufka C, Blaukat A, Pfeffer K, Offermanns S, PUMA-G and HM74 are receptors for nicotinic acid and mediate its anti-lipolytic effect. Nat. Med 9, 352–355 (2003). [PubMed: 12563315]
16. Wise A, Foord SM, Fraser NJ, Barnes AA, Elshourbagy N, Eilert M, Ignar DM, Murdock PR, Steplewski K, Green A, Brown AJ, Dowell SJ, Szekeres PG, Hassall DG, Marshall FH, Wilson S, Pike NB, Molecular identification of high and low affinity receptors for nicotinic acid. J. Biol. Chem 278, 9869–9874 (2003). [PubMed: 12522134]
17. Soga T, Kamohara M, Takasaki J, Matsumoto S, Saito T, Ohishi T, Hiyama H, Matsuo A, Matsushime H, Furuichi K, Molecular identification of nicotinic acid receptor. Biochem. Biophys. Res. Commun 303, 364–369 (2003). [PubMed: 12646212]
18. Giri B, Belanger K, Seamon M, Bradley E, Purohit S, Chong R, Morgan JC, Baban B, Wakade C, Niacin ameliorates neuro-inflammation in Parkinson's disease via GPR109A. Int. J. Mol. Sci 20, 4559 (2019). [PubMed: 31540057]
19. Fu SP, Wang JF, Xue WJ, Liu HM, Liu BR, Zeng YL, Li SN, Huang BX, Lv QK, Wang W, Liu JX, Anti-inflammatory effects of BHBA in both in vivo and in vitro Parkinson's disease models are mediated by GPR109A-dependent mechanisms. J. Neuroinflammation 12, 9 (2015). [PubMed: 25595674]
20. Parodi B, Rossi S, Morando S, Cordano C, Bragoni A, Motta C, Usai C, Wipke BT, Scannevin RH, Mancardi GL, Centonze D, Kerlero de Rosbo N, Uccelli A, Fumarates modulate microglia

activation through a novel HCAR2 signaling pathway and rescue synaptic dysregulation in inflamed CNS. Acta Neuropathol. 130, 279–295 (2015). [PubMed: 25920452]

21. Rawji KS, Young AMH, Ghosh T, Michaels NJ, Mirzaei R, Kappen J, Kolehmainen KL, Alaeiilkhchi N, Lozinski B, Mishra MK, Pu A, Tang W, Zein S, Kaushik DK, Keough MB, Plemel JR, Calvert F, Knights AJ, Gaffney DJ, Tetzlaff W, Franklin RJM, Yong VW, Niacin-mediated rejuvenation of macrophage/microglia enhances remyelination of the aging central nervous system. Acta Neuropathol. 139, 893–909 (2020). [PubMed: 32030468]
22. Sarkar S, Yang R, Mirzaei R, Rawji K, Poon C, Mishra MK, Zemp FJ, Bose P, Kelly J, Dunn JF, Yong VW, Control of brain tumor growth by reactivating myeloid cells with niacin. Sci. Transl. Med 12, eaay9924 (2020). [PubMed: 32238578]
23. Elmore MR, Najafi AR, Koike MA, Dagher NN, Spangenberg EE, Rice RA, Kitazawa M, Matusow B, Nguyen H, West BL, Green KN, Colony-stimulating factor 1 receptor signaling is necessary for microglia viability, unmasking a microglia progenitor cell in the adult brain. Neuron 82, 380–397 (2014). [PubMed: 24742461]
24. Casali BT, MacPherson KP, Reed-Geaghan EG, Landreth GE, Microglia depletion rapidly and reversibly alters amyloid pathology by modification of plaque compaction and morphologies. Neurobiol. Dis 142, 104956 (2020). [PubMed: 32479996]
25. Wang Y, Cella M, Mallinson K, Ulrich JD, Young KL, Robinette ML, Gilfillan S, Krishnan GM, Sudhakar S, Zinselmeyer BH, Holtzman DM, Cirrito JR, Colonna M, TREM2 lipid sensing sustains the microglial response in an Alzheimer's disease model. Cell 160, 1061–1071 (2015). [PubMed: 25728668]
26. Ulland TK, Song WM, Huang SC, Ulrich JD, Sergushichev A, Beatty WL, Loboda AA, Zhou Y, Cairns NJ, Kambal A, Loginicheva E, Gilfillan S, Cella M, Virgin HW, Unanue ER, Wang Y, Artyomov MN, Holtzman DM, Colonna M, TREM2 maintains microglial metabolic fitness in Alzheimer's disease. Cell 170, 649–663.e13 (2017). [PubMed: 28802038]
27. Woodling NS, Wang Q, Priyam PG, Larkin P, Shi J, Johansson JU, Zagol-Ikapitte I, Boutaud O, Andreasson KI, Suppression of Alzheimer-associated inflammation by microglial prostaglandin-E2 EP4 receptor signaling. J. Neurosci 34, 5882–5894 (2014). [PubMed: 24760848]
28. Lukasova M, Malaval C, Gille A, Kero J, Offermanns S, Nicotinic acid inhibits progression of atherosclerosis in mice through its receptor GPR109A expressed by immune cells. J. Clin. Invest 121, 1163–1173 (2011). [PubMed: 21317532]
29. Hanson J, Gille A, Zwykiel S, Lukasova M, Clausen BE, Ahmed K, Tunaru S, Wirth A, Offermanns S, Nicotinic acid- and monomethyl fumarate-induced flushing involves GPR109A expressed by keratinocytes and COX-2-dependent prostanoid formation in mice. J. Clin. Invest 120, 2910–2919 (2010). [PubMed: 20664170]
30. Rahman M, Muhammad S, Khan MA, Chen H, Ridder DA, Muller-Fielitz H, Pokorna B, Vollbrandt T, Stolting I, Nadrowitz R, Okun JG, Offermanns S, Schwaninger M, The β-hydroxybutyrate receptor HCA2 activates a neuroprotective subset of macrophages. Nat. Commun 5, 3944 (2014). [PubMed: 24845831]
31. Reed-Geaghan EG, Croxford AL, Becher B, Landreth GE, Plaque-associated myeloid cells derive from resident microglia in an Alzheimer's disease model. J. Exp. Med 217, e20191374 (2020). [PubMed: 31967645]
32. Wang Y, Ulland TK, Ulrich JD, Song W, Tzaferis JA, Hole JT, Yuan P, Mahan TE, Shi Y, Gilfillan S, Cella M, Grutzendler J, DeMattos RB, Cirrito JR, Holtzman DM, Colonna M, TREM2-mediated early microglial response limits diffusion and toxicity of amyloid plaques. J. Exp. Med 213, 667–675 (2016). [PubMed: 27091843]
33. Krasemann S, Madore C, Cialic R, Baufeld C, Calcagno N, El Fatimy R, Beckers L, O'Loughlin E, Xu Y, Fanek Z, Greco DJ, Smith ST, Tweet G, Humulock Z, Zrzavy T, Conde-Sanroman P, Gacias M, Weng Z, Chen H, Tjon E, Mazaheri F, Hartmann K, Madi A, Ulrich JD, Glatzel M, Worthmann A, Heeren J, Budnik B, Lemere C, Ikezu T, Heppner FL, Litvak V, Holtzman DM, Lassmann H, Weiner HL, Ochando J, Haass C, Butovsky O, The TREM2-APOE pathway drives the transcriptional phenotype of dysfunctional microglia in neurodegenerative diseases. Immunity 47, 566–581.e9 (2017). [PubMed: 28930663]
34. Litvinchuk A, Wan YW, Swartzlander DB, Chen F, Cole A, Propson NE, Wang Q, Zhang B, Liu Z, Zheng H, Complement C3aR inactivation attenuates tau pathology and reverses an immune

network deregulated in tauopathy models and Alzheimer's disease. Neuron 100, 1337–1353.e5 (2018). [PubMed: 30415998]

35. Friedman BA, Srinivasan K, Ayalon G, Meilandt WJ, Lin H, Huntley MA, Cao Y, Lee SH, Haddick PCG, Ngu H, Modrusan Z, Larson JL, Kaminker JS, van der Brug MP, Hansen DV, Diverse brain myeloid expression profiles reveal distinct microglial activation states and aspects of alzheimer's disease not evident in mouse models. Cell Rep. 22, 832–847 (2018). [PubMed: 29346778]
36. Narayanan M, Huynh JL, Wang K, Yang X, Yoo S, McElwee J, Zhang B, Zhang C, Lamb JR, Xie T, Suver C, Molony C, Melquist S, Johnson AD, Fan G, Stone DJ, Schadt EE, Casaccia P, Emilsson V, Zhu J, Common dysregulation network in the human prefrontal cortex underlies two neurodegenerative diseases. Mol. Syst. Biol 10, 743 (2014). [PubMed: 25080494]
37. Zhang Y, Sloan SA, Clarke LE, Caneda C, Plaza CA, Blumenthal PD, Vogel H, Steinberg GK, Edwards MS, Li G, Duncan JA 3rd, Cheshier SH, Shuer LM, Chang EF, Grant GA, Gephart MG, Barres BA, Purification and characterization of progenitor and mature human astrocytes reveals transcriptional and functional differences with mouse. Neuron 89, 37–53 (2016). [PubMed: 26687838]
38. Zhang Y, Chen K, Sloan SA, Bennett ML, Scholze AR, O'Keeffe S, Phatnani HP, Guarnieri P, Caneda C, Ruderisch N, Deng S, Liddelow SA, Zhang C, Daneman R, Maniatis T, Barres BA, Wu JQ, An RNA-sequencing transcriptome and splicing database of glia, neurons, and vascular cells of the cerebral cortex. J. Neurosci 34, 11929–11947 (2014). [PubMed: 25186741]
39. Galatro TF, Holtman IR, Lerario AM, Vainchtein ID, Brouwer N, Sola PR, Veras MM, Pereira TF, Leite REP, Moller T, Wes PD, Sogayar MC, Laman JD, den Dunnen W, Pasqualucci CA, Oba-Shinjo SM, Boddeke E, Marie SKN, Eggen BJL, Transcriptomic analysis of purified human cortical microglia reveals age-associated changes. Nat. Neurosci 20, 1162–1171 (2017). [PubMed: 28671693]
40. Long JM, Holtzman DM, Alzheimer disease: An update on pathobiology and treatment strategies. Cell 179, 312–339 (2019). [PubMed: 31564456]
41. Oakley H, Cole SL, Logan S, Maus E, Shao P, Craft J, Guillozet-Bongaarts A, Ohno M, Disterhoft J, Van Eldik L, Berry R, Vassar R, Intraneuronal beta-amyloid aggregates, neurodegeneration, and neuron loss in transgenic mice with five familial Alzheimer's disease mutations: Potential factors in amyloid plaque formation. J. Neurosci 26, 10129–10140 (2006). [PubMed: 17021169]
42. Daria A, Colombo A, Llovera G, Hampel H, Willem M, Liesz A, Haass C, Tahirovic S, Young microglia restore amyloid plaque clearance of aged microglia. EMBO J. 36, 583–603 (2017). [PubMed: 28007893]
43. Liu Z, Condello C, Schain A, Harb R, Grutzendler J, CX3CR1 in microglia regulates brain amyloid deposition through selective protofibrillar amyloid-β phagocytosis. J. Neurosci 30, 17091–17101 (2010). [PubMed: 21159979]
44. Smith AM, Gibbons HM, Oldfield RL, Bergin PM, Mee EW, Curtis MA, Faull RL, Dragunow M, M-CSF increases proliferation and phagocytosis while modulating receptor and transcription factor expression in adult human microglia. J. Neuroinflammation 10, 85 (2013). [PubMed: 23866312]
45. Tejera D, Heneka MT, In vivo phagocytosis analysis of amyloid beta. Methods Mol. Biol 2034, 287–292 (2019). [PubMed: 31392693]
46. Yuan P, Condello C, Keene CD, Wang Y, Bird TD, Paul SM, Luo W, Colonna M, Baddeley D, Grutzendler J, TREM2 haplodeficiency in mice and humans impairs the microglia barrier function leading to decreased amyloid compaction and severe axonal dystrophy. Neuron 90, 724–739 (2016). [PubMed: 27196974]
47. Benzing WC, Mufson EJ, Armstrong DM, Alzheimer's disease-like dystrophic neurites characteristically associated with senile plaques are not found within other neurodegenerative diseases unless amyloid beta-protein deposition is present. Brain Res. 606, 10–18 (1993). [PubMed: 8096426]
48. Cheng-Hathaway PJ, Reed-Geaghan EG, Jay TR, Casali BT, Bemiller SM, Puntambekar SS, von Saucken VE, Williams RY, Karlo JC, Moutinho M, Xu G, Ransohoff RM, Lamb BT, Landreth GE, The Trem2 R47H variant confers loss-of-function-like phenotypes in Alzheimer's disease. Mol. Neurodegener 13, 29 (2018). [PubMed: 29859094]

49. Condello C, Yuan P, Schain A, Grutzendler J, Microglia constitute a barrier that prevents neurotoxic protofibrillar Aβ42 hotspots around plaques. Nat. Commun 6, 6176 (2015). [PubMed: 25630253]
50. Bhattacharya S, Haertel C, Maelicke A, Montag D, Galantamine slows down plaque formation and behavioral decline in the 5XFAD mouse model of Alzheimer's disease. PLOS ONE 9, e89454 (2014). [PubMed: 24586789]
51. He Z, Yang Y, Xing Z, Zuo Z, Wang R, Gu H, Qi F, Yao Z, Intraperitoneal injection of IFN-γ restores microglial autophagy, promotes amyloid-β clearance and improves cognition in APP/PS1 mice. Cell Death Dis. 11, 440 (2020). [PubMed: 32514180]
52. Mastrangelo MA, Sudol KL, Narrow WC, Bowers WJ, Interferon-{gamma} differentially affects Alzheimer's disease pathologies and induces neurogenesis in triple transgenic-AD mice. Am. J. Pathol 175, 2076–2088 (2009). [PubMed: 19808651]
53. Keren-Shaul H, Spinrad A, Weiner A, Matcovitch-Natan O, Dvir-Szternfeld R, Ulland TK, David E, Baruch K, Lara-Astaiso D, Toth B, Itzkovitz S, Colonna M, Schwartz M, Amit I, A unique microglia type associated with restricting development of Alzheimer's disease. Cell 169, 1276–1290.e17 (2017). [PubMed: 28602351]
54. Sala Frigerio C, Wolfs L, Fattorelli N, Thrupp N, Voytyuk I, Schmidt I, Mancuso R, Chen WT, Woodbury ME, Srivastava G, Moller T, Hudry E, Das S, Saido T, Karran E, Hyman B, Perry VH, Fiers M, De Strooper B, The major risk factors for Alzheimer's disease: Age, sex, and genes modulate the microglia response to abeta plaques. Cell Rep. 27, 1293–1306.e6 (2019). [PubMed: 31018141]
55. McAlpine CS, Park J, Griciuc A, Kim E, Choi SH, Iwamoto Y, Kiss MG, Christie KA, Vinegoni C, Poller WC, Mindur JE, Chan CT, He S, Janssen H, Wong LP, Downey J, Singh S, Anzai A, Kahles F, Jorfi M, Feruglio PF, Sadreyev RI, Weissleder R, Kleinstiver BP, Nahrendorf M, Tanzi RE, Swirski FK, Astrocytic interleukin-3 programs microglia and limits Alzheimer's disease. Nature 595, 701–706 (2021). [PubMed: 34262178]
56. Gratuze M, Chen Y, Parhizkar S, Jain N, Strickland MR, Serrano JR, Colonna M, Ulrich JD, Holtzman DM, Activated microglia mitigate Aβ-associated tau seeding and spreading. J. Exp. Med 218, e20210542 (2021). [PubMed: 34100905]
57. Wang S, Mustafa M, Yuede CM, Salazar SV, Kong P, Long H, Ward M, Siddiqui O, Paul R, Gilfillan S, Ibrahim A, Rhinn H, Tassi I, Rosenthal A, Schwabe T, Colonna M, Anti-human TREM2 induces microglia proliferation and reduces pathology in an Alzheimer's disease model. J. Exp. Med 217, e20200785 (2020). [PubMed: 32579671]
58. Schlepckow K, Monroe KM, Kleinberger G, Cantuti-Castelvetri L, Parhizkar S, Xia D, Willem M, Werner G, Pettkus N, Brunner B, Sulzen A, Nuscher B, Hampel H, Xiang X, Feederle R, Tahirovic S, Park JI, Prorok R, Mahon C, Liang CC, Shi J, Kim DJ, Sabelstrom H, Huang F, Di Paolo G, Simons M, Lewcock JW, Haass C, Enhancing protective microglial activities with a dual functionTREM2 antibody to the stalk region. EMBO Mol. Med 12, e11227 (2020). [PubMed: 32154671]
59. Price BR, Sudduth TL, Weekman EM, Johnson S, Hawthorne D, Woolums A, Wilcock DM, Therapeutic Trem2 activation ameliorates amyloid-beta deposition and improves cognition in the 5XFAD model of amyloid deposition. J. Neuroinflammation 17, 238 (2020). [PubMed: 32795308]
60. Kos Pharmaceuticals, NIASPAN, www.accessdata.fda.gov/drugsatfda_docs/label/2005/020381s020lbl.pdf.
61. Zhang J, Chen J, Li Y, Cui X, Zheng X, Roberts C, Lu M, Elias SB, Chopp M, Niaspan treatment improves neurological functional recovery in experimental autoimmune encephalomyelitis mice. Neurobiol. Dis 32, 273–280 (2008). [PubMed: 18778774]
62. Bolkent S, Yanardag R, Bolkent S, Doger MM, Beneficial effects of combined treatment with niacin and chromium on the liver of hyperlipemic rats. Biol. Trace Elem. Res 101, 219–230 (2004). [PubMed: 15564652]
63. Lauring B, Taggart AK, Tata JR, Dunbar R, Caro L, Cheng K, Chin J, Colletti SL, Cote J, Khalilieh S, Liu J, Luo WL, Maclean AA, Peterson LB, Polis AB, Sirah W, Wu TJ, Liu X, Jin L, Wu K, Boatman PD, Semple G, Behan DP, Connolly DT, Lai E, Wagner JA, Wright SD, Cuffie C, Mitchel YB, Rader DJ, Paolini JF, Waters MG, Plump A, Niacin lipid efficacy is independent of

both the niacin receptor GPR109A and free fatty acid suppression. Sci. Transl. Med 4, 148ra115 (2012).

64. Nair AB, Jacob S, A simple practice guide for dose conversion between animals and human. J. Basic Clin. Pharm 7, 27–31 (2016). [PubMed: 27057123]
65. Song WL, FitzGerald GA, Niacin, an old drug with a new twist. J. Lipid Res 54, 2586–2594 (2013). [PubMed: 23948546]
66. Lai E, De Lepeleire I, Crumley TM, Liu F, Wenning LA, Michiels N, Vets E, O'Neill G, Wagner JA, Gottesdiener K, Suppression of niacin-induced vasodilation with an antagonist to prostaglandin D2 receptor subtype 1. Clin. Pharmacol. Ther 81, 849–857 (2007). [PubMed: 17392721]
67. Wakade C, Giri B, Malik A, Khodadadi H, Morgan JC, Chong RK, Baban B, Niacin modulates macrophage polarization in Parkinson's disease. J. Neuroimmunol 320, 76–79 (2018). [PubMed: 29759143]
68. Wakade C, Chong R, Bradley E, Morgan JC, Low-dose niacin supplementation modulates GPR109A, niacin index and ameliorates Parkinson's disease symptoms without side effects. Clin. Case Rep 3, 635–637 (2015). [PubMed: 26273459]
69. Carretta MD, Barria Y, Borquez K, Urra B, Rivera A, Alarcon P, Hidalgo MA, Burgos RA, beta-hydroxybutyrate and hydroxycarboxylic acid receptor 2 agonists activate the AKT, ERK and AMPK pathways, which are involved in bovine neutrophil chemotaxis. Sci. Rep 10, 12491 (2020). [PubMed: 32719460]
70. Li Z, Li X, Lin S, Chen Y, Ma S, Fu Y, Wei C, Xu W, Nicotinic acid receptor GPR109A exerts anti-inflammatory effects through inhibiting the Akt/mTOR signaling pathway in MIN6 pancreatic β cells. Ann. Clin. Lab. Sci 47, 729–737 (2017). [PubMed: 29263047]
71. Geng HW, Yin FY, Zhang ZF, Gong X, Yang Y, Butyrate suppresses glucose metabolism of colorectal cancer cells via GPR109a-AKT signaling pathway and enhances chemotherapy. Front. Mol. Biosci 8, 634874 (2021). [PubMed: 33855046]
72. Ye L, Cao Z, Lai X, Shi Y, Zhou N, Niacin ameliorates hepatic steatosis by inhibiting de novo lipogenesis via a GPR109A-mediated PKC-ERK1/2-AMPK signaling pathway in C57BL/6 mice fed a high-fat diet. J. Nutr 150, 672–684 (2020). [PubMed: 31858105]
73. Gaidarov I, Chen X, Anthony T, Maciejewski-Lenoir D, Liaw C, Unett DJ, Differential tissue and ligand-dependent signaling of GPR109A receptor: Implications for anti-atherosclerotic therapeutic potential. Cell. Signal 25, 2003–2016 (2013). [PubMed: 23770183]
74. Cramer PE, Cirrito JR, Wesson DW, Lee CY, Karlo JC, Zinn AE, Casali BT, Restivo JL, Goebel WD, James MJ, Brunden KR, Wilson DA, Landreth GE, ApoE-directed therapeutics rapidly clear β-amyloid and reverse deficits in AD mouse models. Science 335, 1503–1506 (2012). [PubMed: 22323736]
75. Mariani MM, Malm T, Lamb R, Jay TR, Neilson L, Casali B, Medarametla L, Landreth GE, Neuronally-directed effects of RXR activation in a mouse model of Alzheimer's disease. Sci. Rep 7, 42270 (2017). [PubMed: 28205585]
76. Casali BT, Corona AW, Mariani MM, Karlo JC, Ghosal K, Landreth GE, Omega-3 fatty acids augment the actions of nuclear receptor agonists in a mouse model of Alzheimer's disease. J. Neurosci 35, 9173–9181 (2015). [PubMed: 26085639]
77. Radde R, Bolmont T, Kaeser SA, Coomaraswamy J, Lindau D, Stoltze L, Calhoun ME, Jaggi F, Wolburg H, Gengler S, Haass C, Ghetti B, Czech C, Holscher C, Mathews PM, Jucker M, Abeta42-driven cerebral amyloidosis in transgenic mice reveals early and robust pathology. EMBO Rep. 7, 940–946 (2006). [PubMed: 16906128]
78. Mahi NA, Najafabadi MF, Pilarczyk M, Kouril M, Medvedovic M, GREIN: An interactive web platform for re-analyzing GEO RNA-seq data. Sci. Rep 9, 7580 (2019). [PubMed: 31110304]
79. Tsai AP, Lin PB, Dong C, Moutinho M, Casali BT, Liu Y, Lamb BT, Landreth GE, Oblak AL, Nho K, INPP5D expression is associated with risk for Alzheimer's disease and induced by plaque-associated microglia. Neurobiol. Dis 153, 105303 (2021). [PubMed: 33631273]
80. Saura J, Tusell JM, Serratosa J, High-yield isolation of murine microglia by mild trypsinization. Glia 44, 183–189 (2003). [PubMed: 14603460]

81. Koenigsknecht J, Landreth G, Microglial phagocytosis of fibrillar beta-amyloid through a beta1 integrin-dependent mechanism. J. Neurosci 24, 9838–9846 (2004). [PubMed: 15525768]

82. Puntambekar SS, Hinton DR, Yin X, Savarin C, Bergmann CC, Trapp BD, Stohlman SA, Interleukin-10 is a critical regulator of white matter lesion containment following viral induced demyelination. Glia 63, 2106–2120 (2015). [PubMed: 26132901]

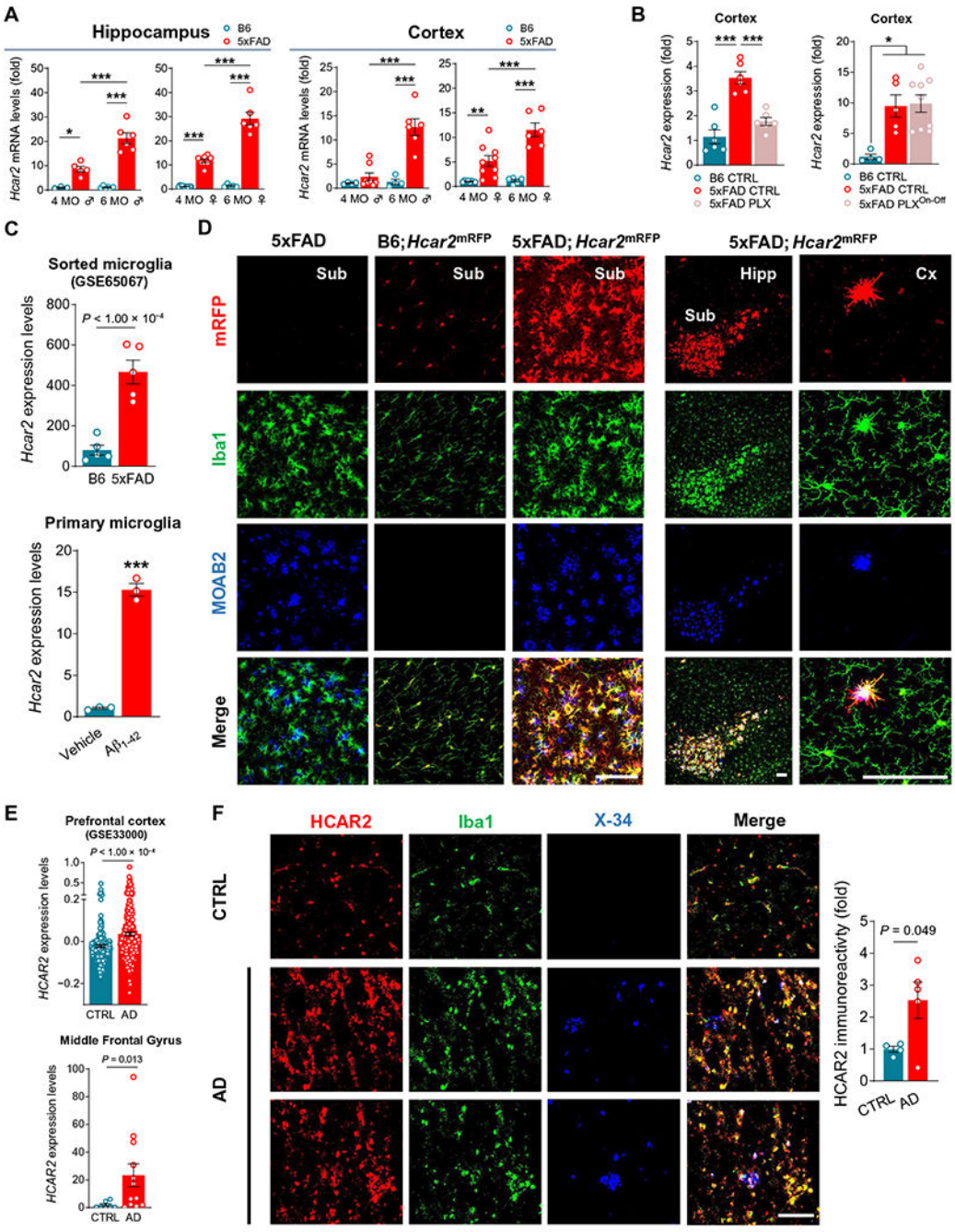

Fig. 1. Induction of HCAR2 by microglia in AD.

(**A**) qPCR analysis of *Hcar2* expression in the hippocampus and cortex of 4- and 6-month-old male (♂) and female (♀) nontransgenic control (B6) and 5xFAD animals (n♂ = 3 to 8; n♀ = 5 to 12 per group). Statistical analysis was performed by two-way ANOVA ($P^{int} < 0.001$) followed by Tukey's post hoc test. (**B**) qPCR analysis of *Hcar2* expression in the cortex of 4-month-old 5xFAD mice treated with the CSFR1 antagonist PLX5622 (PLX) for 28 days (n = 4 to 9 per group) (left) and discontinued from PLX for 28 more days (On-Off; n = 6 per group) (right). Statistical analysis was performed by one-way

ANOVA ($P < 0.001$) followed by Tukey's post hoc test (left) and Kruskal-Wallis test ($P < 0.01$) followed by Dunn's test (right). (**C**) *Hcar2* expression data obtained from a dataset of sorted microglia from the brains of 5-month-old B6 and 5xFAD mice ($n = 5$ per genotype) (GSE65067) (top). qPCR analysis of *Hcar2* expression in murine primary microglia cultures incubated with 5 μM $A\beta_{1\text{-}42}$ aggregates for 24 hours ($n = 3$ per group) (bottom). Statistical analysis was performed by Student's *t* test. (**D**) Visualization of *Hcar2* induction (mRFP-red) with immunohistochemistry (IHC) staining for Iba1 (green) and amyloid plaques (MOAB2-blue) in the subiculum (Sub), Hippocampus (Hipp), and Cortex (Cx) of B6 and 5xFAD;*Hcar2*^{mRFP} mice. Scale bars, 100 μm. (**E**) *HCAR2* expression obtained from a human transcriptomic dataset of dorsolateral prefrontal cortex (BA9) tissue of 157 nondemented controls and 310 patients with AD (GSE33000) (top). qPCR analysis of *HCAR2* in postmortem middle frontal gyrus tissue of 7 control (CTRL) and 12 patients with AD (bottom). Statistical analysis was performed by Mann-Whitney test (bottom). (**F**) IHC for HCAR2 (red), Iba1 (green), and plaques (X-34-blue) in human CTRL and AD brain and quantification of HCAR2 immunoreactivity ($n = 4$ to 5 per group). Scale bar, 100 μm. Microarray datasets GSE65067 and GSE33000 were analyzed using the GEO2R online tool (www.ncbi.nlm.nih.gov/geo/geo2r/). Data are expressed as mean values ± SEM (*$P < 0.05$, **$P < 0.01$ and ***$P < 0.001$).

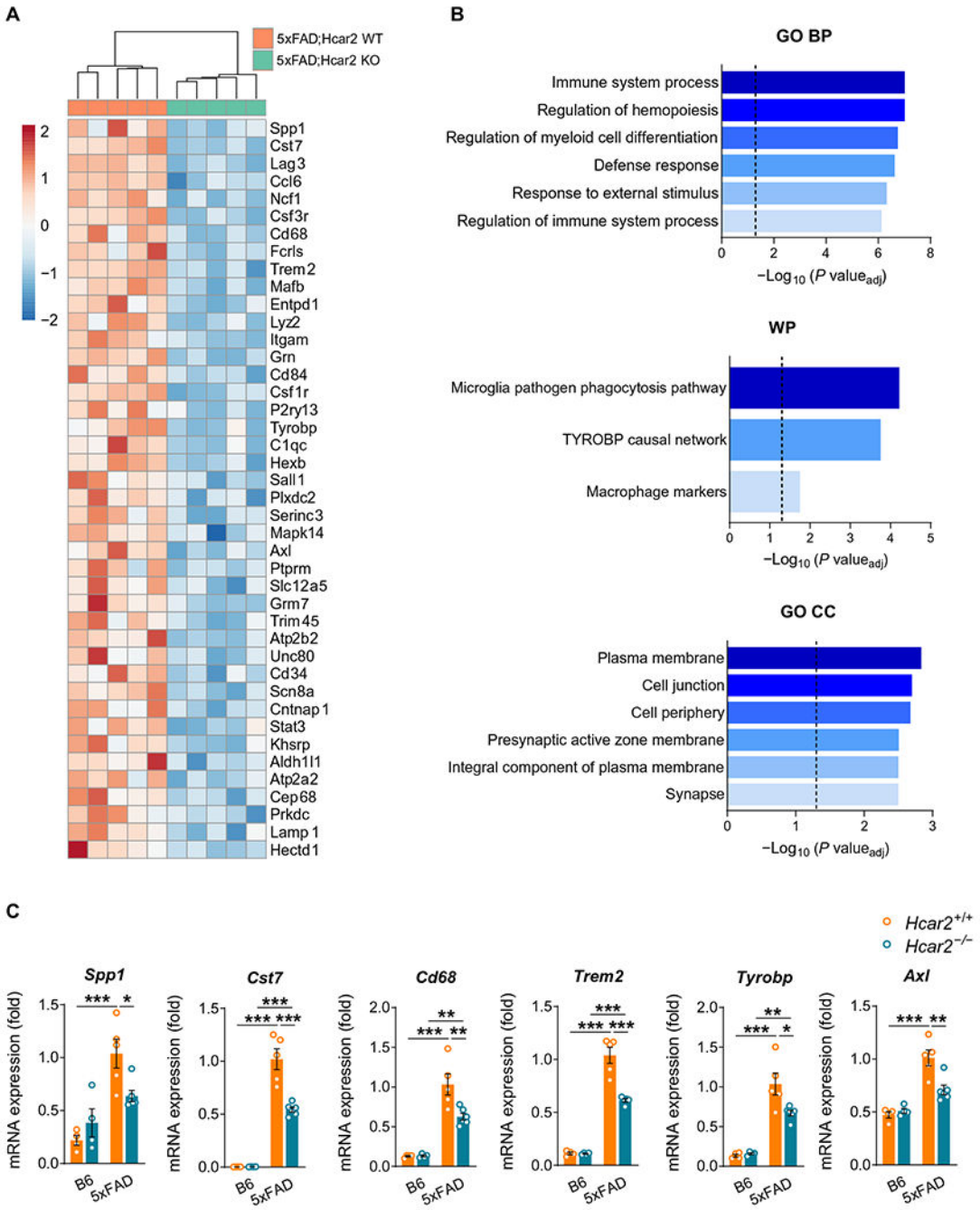

Fig. 2. Lack of *Hcar2* disrupts microglial pathways in the amyloidogenic 5xFAD brain.

(**A**) Gene expression heatmap of differentially expressed genes (DEGs) (adj. $P < 0.05$) between the hippocampus of 6-month-old female 5xFAD;*Hcar2*$^{+/+}$ and 5xFAD;*Hcar2*$^{-/-}$ mice analyzed by the nCounter Glial Profiling Panel from NanoString ($n = 5$ per genotype). ClustVis software (https://biit.cs.ut.ee/clustvis/) was used to perform clustering and generate the heatmap. Clustering used Euclidean distance and average linkage. Data were subjected to centering and unit variance scaling (z scores). (**B**) Top 6 Gene Ontology terms for Biological Process (GO BP) (top graph), WikiPathways (WP) analysis (middle graph), and

top 6 GO terms for Cellular Component (GO CC) (bottom graph), using DEGs from (A) and threshold of adj. $P < 0.05$ (dashed line). (**C**) qPCR analysis of several DEGs from (A) in hippocampus of B6 and 5xFAD *Hcar2*$^{+/+}$, as well as B6 and 5xFAD *Hcar2*$^{-/-}$ animals (n = 4 to 6 per genotype). Statistical analysis was performed by two-way ANOVA ($P^{int} < 0.05$) followed by Tukey's post hoc test. Data are expressed as mean values ± SEM (*$P < 0.05$, **$P < 0.01$, and ***$P < 0.001$).

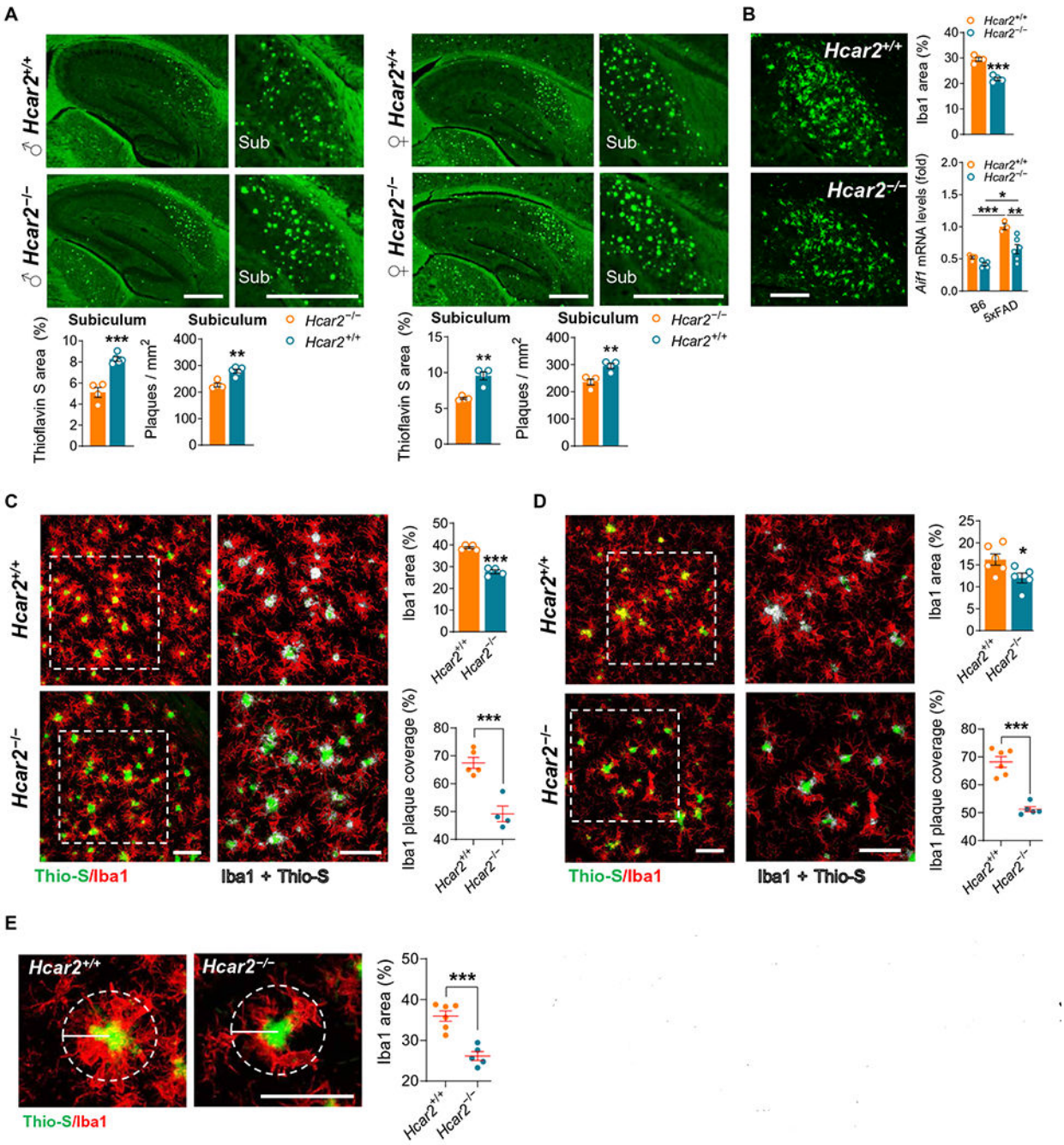

Fig. 3. Lack of *Hcar2* curtails microglia engagement with plaques and increases plaque burden.

(**A**) IHC staining of amyloid plaques with thioflavin S (Thio-S; green) and quantification of thioflavin S percent area and plaque number in brain tissue of 4-month-old male (♂) and female (♀) 5xFAD;*Hcar2*$^{+/+}$ and 5xFAD;*Hcar2*$^{-/-}$ mice (n♂ = 4 to 5; n♀ = 4 per genotype). Subiculum (Sub) is magnified on the right. Statistical analysis was performed by Student's *t* test. Scale bars, 500 μm. (**B**) IHC staining for Iba1 (green) in the subiculum of 4-month-old female 5xFAD;*Hcar2*$^{+/+}$ and 5xFAD;*Hcar2*$^{-/-}$ mice and quantification of total Iba1 area in subiculum (left graph) (n = 4 per genotype). qPCR analysis of *Aif1* expression in the

hippocampus of B6 and 5xFAD *Hcar2*$^{+/+}$ and B6 and 5xFAD *Hcar2*$^{-/-}$ mice (n = 3 to 6 per genotype). Statistical analysis was performed by Student's t test for Iba1 area and by two way ANOVA ($P^{int} < 0.05$) followed by Tukey's post hoc test for *Aif1* expression. Scale bar, 200 μm. (**C**) IHC staining for Iba1 (red) and Thio-S^{+} amyloid plaques in the subiculum of 6-month-old female 5xFAD;*Hcar2*$^{+/+}$ and 5xFAD;*Hcar2*$^{-/-}$ mice. Total Iba1 area in subiculum was quantified (top graph). Iba1 coverage of Thio-S^{+} plaques can be visualized by the color gray in the right IHC panel. Iba1 coverage of plaques were quantified and averaged per animal (bottom graph) (n = 4 to 5 mice and >200 plaques per genotype). Statistical analysis was performed by Student's t test. Scale bars, 50 μm. (**D**) IHC staining for Iba1 (red) and Thio-S^{+} amyloid plaques in the cortex of 6-month-old female 5xFAD;*Hcar2*$^{+/+}$ and 5xFAD;*Hcar2*$^{-/-}$ mice. Total Iba1 area in subiculum was quantified (top graph). Iba1 coverage of Thio-S^{+} plaques can be visualized by the color gray in the right IHC panel. Iba1 coverage of plaques were quantified and averaged per animal (bottom graph) (n = 5 to 6 mice and >100 plaques per genotype). Statistical analysis was performed by Student's t test. Scale bars, 50 μm. (**E**) IHC staining of Iba1 (red) and Thio-S^{+} amyloid plaques in the subiculum of 6-month-old female 5xFAD;*Hcar2*$^{+/+}$ and 5xFAD;*Hcar2*$^{-/-}$ mice. Iba1 coverage was quantified within a circular area with a radius of 25 μm centered on thioflavin S–positive plaques (n = 5 to 6 mice and >100 plaques per genotype). Statistical analysis was performed by Student's t test. Scale bar, 50 μm. Data are expressed as mean values ± SEM (*$P < 0.05$, **$P < 0.01$, and ***$P < 0.001$).

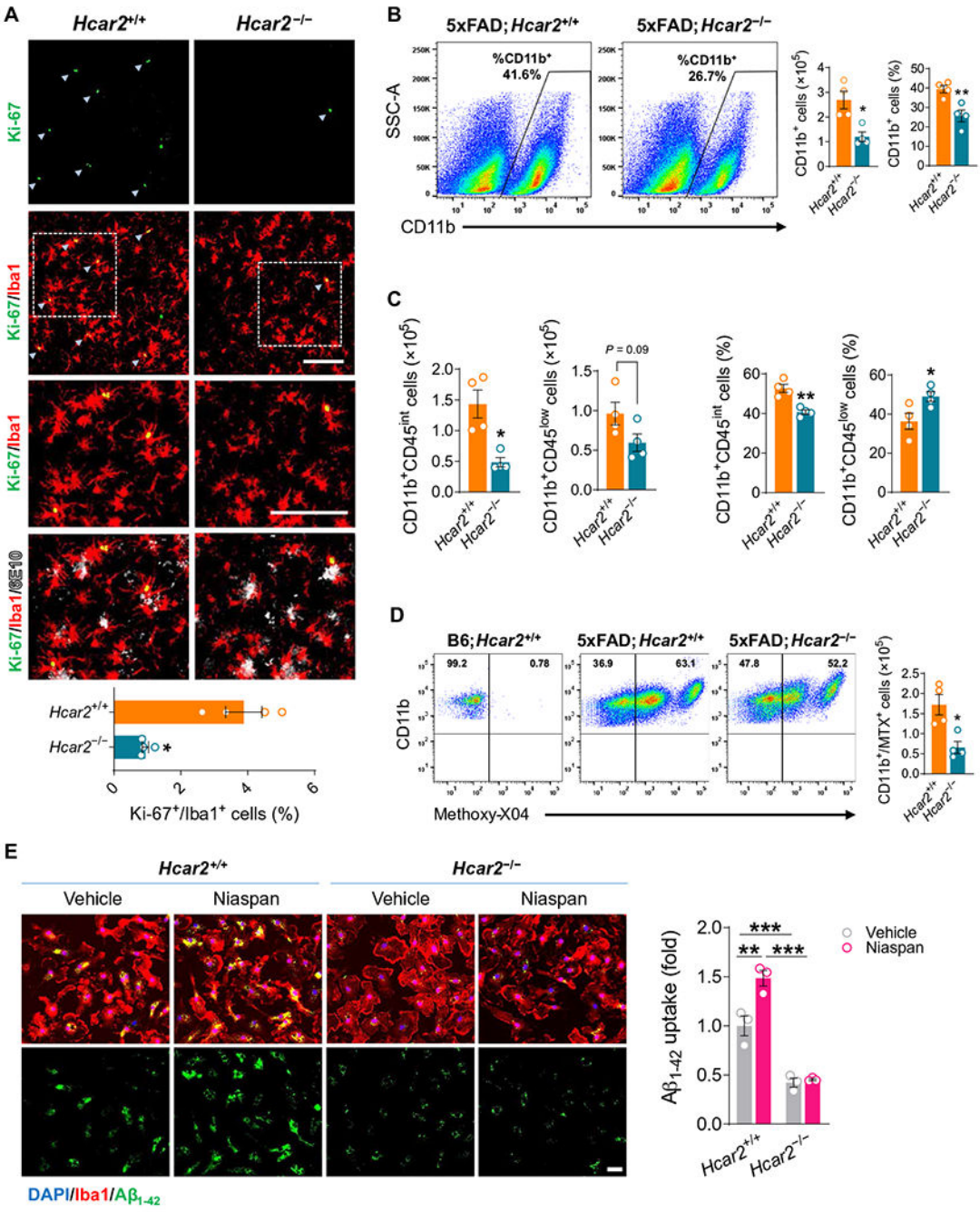

Fig. 4. *Hcar2* is required for efficient microglia proliferation and amyloid uptake.

(**A**) IHC for the proliferation marker Ki-67 (green), Iba1 (red), and Aβ (6E10; gray) in the cortex of 4-month-old female 5xFAD;*Hcar2*$^{+/+}$ and 5xFAD;*Hcar2*$^{-/-}$ mice. The percent of Ki-67–positive microglia (Ki-67^{+}/Iba1^{+}) cells within the total microglia population (Iba1^{+}) was determined (n = 4 per genotype). Statistical analysis was performed by Mann-Whitney test. Scale bars, 100 μm. (**B** to **D**) Brain tissue of 6-month-old female 5xFAD;*Hcar2*$^{+/+}$ and 5xFAD;*Hcar2*$^{-/-}$ mice previously injected intraperitoneally with methoxy-X04 were analyzed by flow cytometry. Microglia cells were stained with CD11b-PeCy7- and CD45-

FITC–conjugated antibodies. (B) The number and percent of CD11b-positive ($CD11b^+$) microglia cells were determined and (C) the number and percent of CD45-intermediate ($CD45^{int}$) and CD45-low ($CD45^{low}$) within the $CD11b^+$ microglia population ($CD11b^+/CD45^{int}$ and $CD11b^+/CD45^{low}$). (D) The number of methoxy-X04–positive (MTX^+) cells within the $CD11b^+$ microglia population ($CD11b^+/MTX^+$) was also analyzed ($n = 4$ per genotype). Statistical analysis was performed by Mann-Whitney test for the number of $CD11b^+/CD45^{int}$. For the rest of the data, Student *t* test was performed. SSC-A, side scatter area. (**E**) Immunofluorescence of primary murine microglia from $Hcar2^{+/+}$ and $Hcar2^{-/-}$ mice incubated with Niaspan for 24 hours followed by a 30-min incubation with aggregates of fluorescently labeled $A\beta_{1\text{-}42}$ (green). Cells were stained with 4',6-diamidino-2-phenylindole (DAPI; nuclei staining, blue) and Iba1 (red). Scale bar, 25 μm. Quantification of $A\beta_{1\text{-}42}$ uptake by analyzing fluorescence per cell of at least 600 cells for each condition ($n = 3$ per condition). Statistical analysis was performed by two-way ANOVA ($P^{int} < 0.05$) followed by Tukey's post hoc test. Scale bar, 25 μM. Data are expressed as mean values ± SEM (*$P < 0.05$, **$P < 0.01$, and ***$P < 0.001$).

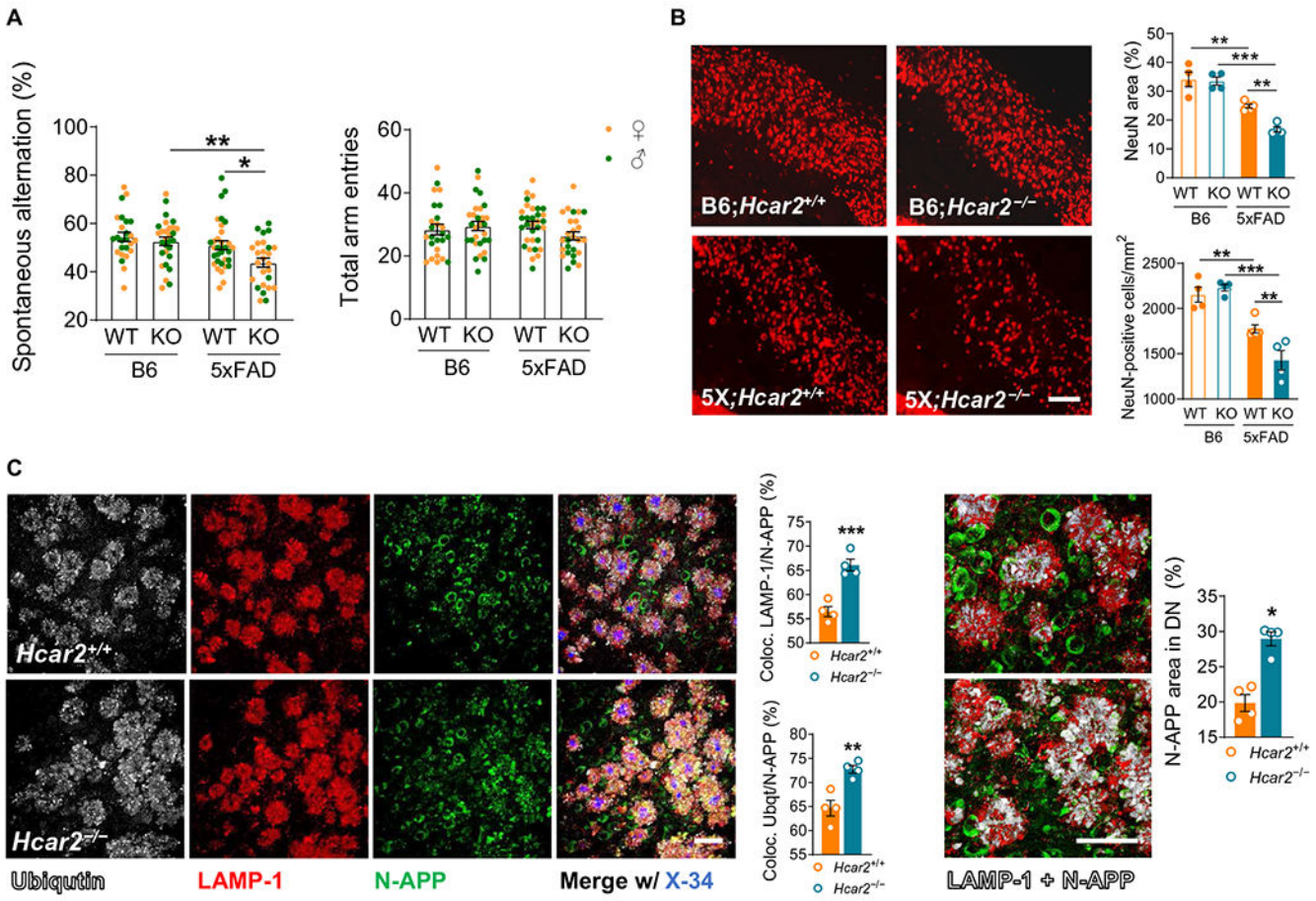

Fig. 5. Lack of *Hcar2* exacerbates amyloid-associated neuropathology.

(**A**) Working memory of 4-month-old male (♂; green) and female (♀; yellow) B6 and 5xFAD *Hcar2*$^{+/+}$, as well as B6 and 5xFAD *Hcar2*$^{-/-}$ mice assessed by percent of spontaneous alternation in the Y-maze task. Total arm entries were also analyzed. (n = 25 to 32 mice per genotype). Statistical analysis was performed by two-way ANOVA for spontaneous alternation ($P^{\text{int}} = 0.1514$; $P^{Hcar2\text{genotype}} < 0.05$; $p^{\text{ADgenotype}} < 0.01$) and total arm entries ($P^{\text{int}} = 0.1027$; $p^{Hcar2\text{genotype}} = 0.42$; $p^{\text{ADgenotype}} = 0.547$) followed by Tukey's post hoc test. (**B**) IHC for NeuN (neurons; red) in subiculum of 4-month-old female B6 and 5xFAD *Hcar2*$^{+/+}$ as well as B6 and 5xFAD *Hcar2*$^{-/-}$ mice. Quantification of the number of NeuN-positive cells and total area of NeuN staining within the subiculum (n = 4 to 5 per genotype). Statistical analysis was performed by two-way ANOVA ($P^{\text{int}} < 0.05$) followed by Tukey's post hoc test. Scale bar, 100 μm. (**C**) IHC for ubiquitin (Ubqt), LAMP-1, and N-terminal APP (N-APP) to visualize DNs and X-34 to stain for amyloid plaques in the subiculum of 4-month-old female 5xFAD;*Hcar2*$^{+/+}$ and 5xFAD;*Hcar2*$^{-/-}$ mice. Percent of colocalization of LAMP-1 and Ubqt with N-APP was analyzed (left graphs). Visualization of N-APP staining colocalized with DNs (LAMP-1 positive) (gray) in the right panel. The percent area of N-APP staining within LAMP-1–positive DN was quantified and averaged per animal (n = 4 mice and >200 DN per genotype). Statistical analysis was performed by Student's t test for colocalization data and Mann-Whitney test for N-APP percent area in DN. Scale bar, 50

μm. Data are expressed as mean values ± SEM (*$P < 0.05$, **$P < 0.01$, and ***$P < 0.001$). WT, wild type; KO, knockout.

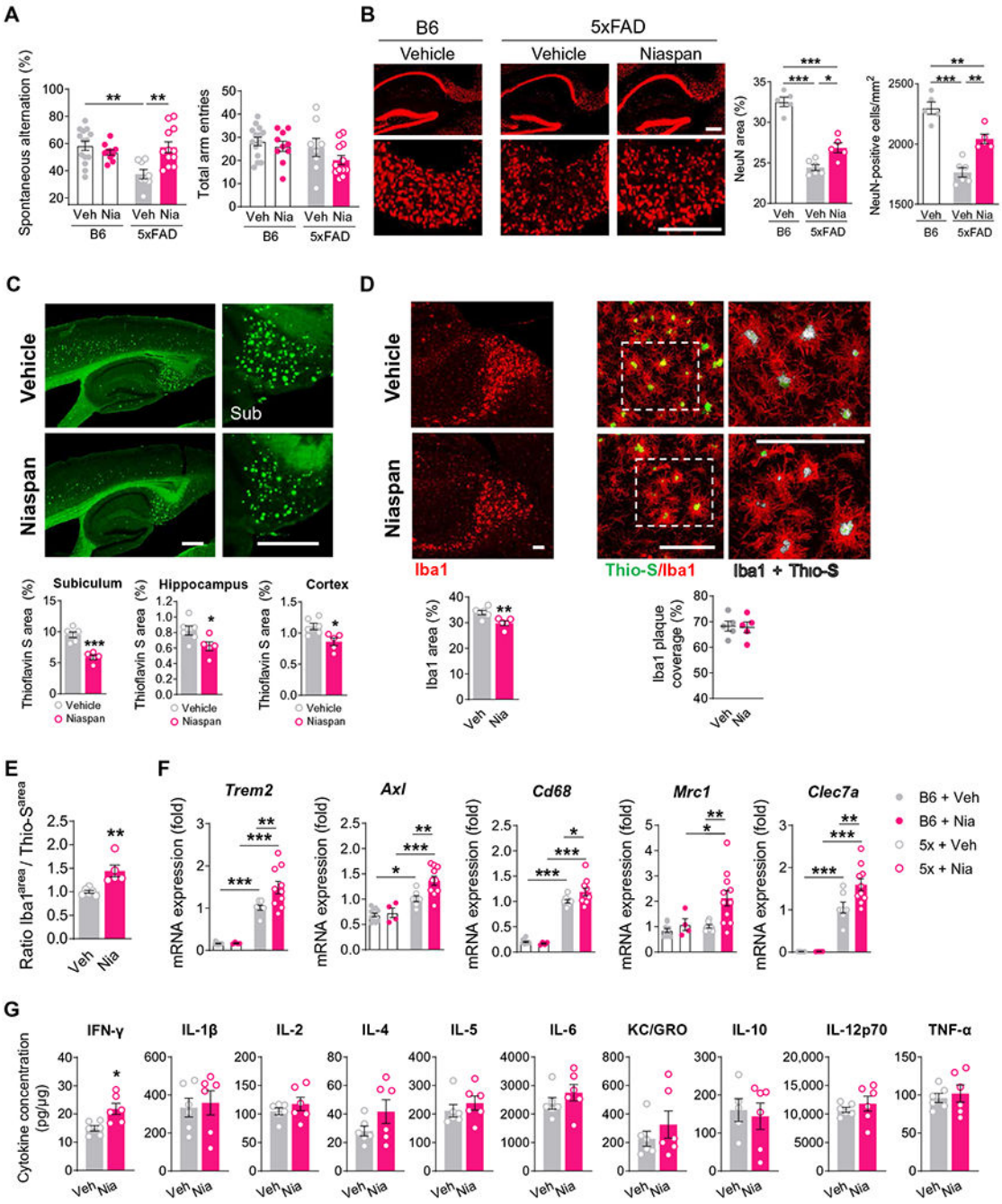

Fig. 6. Niaspan stimulates microglia response and reduces amyloid pathology in AD mice

(**A**) Working memory of 6-month-old male B6 and 5xFAD mice treated with vehicle (Veh) or Niaspan (Nia) assessed by percent of spontaneous alternation in the Y-maze task. Total arms entries were also analyzed (n = 8 to 14 mice per group). Statistical analysis was performed by two-way ANOVA for spontaneous alternation ($P^{int} < 0.01$) and total arm entries ($P^{int} = 0.491$; $P^{treatment} = 0.123$; $P^{genotype} = 0.084$) followed by Tukey's post hoc test. (**B**) IHC for NeuN (neurons; red) in hippocampus of 6-month-old male B6 and 5xFAD mice treated with vehicle or Niaspan with magnification of subiculum area (bottom).

Quantification of total area of NeuN staining and number of NeuN-positive cells and within the subiculum (n = 5 to 6 per group). Scale bars, 250 μm. (**C**) IHC staining of amyloid plaques with thioflavin S and quantification of thioflavin S percent and plaque number in the subiculum, hippocampus, and cortex of 6-month-old male 5xFAD mice treated with vehicle or Niaspan. Subiculum (Sub) is magnified on the right (n = 5 to 6 per group). Statistical analysis was performed by one-way ANOVA ($P < 0.001$) followed by Tukey's post hoc test. Scale bars, 500 μm. (**D**) IHC staining for Iba1 (red) and amyloid plaques (thioflavin S; green) in the subiculum of 6-month-old male 5xFAD mice treated with vehicle (Veh) or Niaspan (Nia). Total Iba1 area in subiculum was quantified (left graph) (n = 5 to 6 per group). Iba1 coverage of thioflavin S–positive plaques can be visualized by the color gray in the right IHC panel. Iba1 coverage of plaques were quantified and averaged per animal (right graph) (n = 5 mice and >200 plaques per group). Scale bars, 100 μm. Statistical analysis was performed by Student's t test. (**E**) Ratio of Iba1 and thioflavin S (Thio-S) areas within the subiculum of 5xFAD animals treated with vehicle (Veh) or Niaspan (Nia) (n = 5 to 6 per group). Statistical analysis was performed by Mann-Whitney test. (**F**) Expression analysis by qPCR of several genes implicated in HCAR2 signaling and AD pathology in the hippocampus of male B6 and 5xFAD mice treated with vehicle and Niaspan (n = 4 to 13 per group). Statistical analysis was performed by two-way ANOVA ($P^{int} < = 0.0767$; $P^{treatment} < 0.05 = 0.0767$; $P^{treatment} < 0.05$; $P^{genotype} = 0.084$) followed by Tukey's post hoc test. (**G**) Cytokine concentration in cortical tissue of 5xFAD mice treated with vehicle or Niaspan (n = 6 per group) quantified by the MSD V-PLEX Plus Proinflammatory Panel 1 Mouse Kit. Statistical analysis was performed by Student's t test. Data are expressed as mean values ± SEM (*$P < 0.05$, **$P < 0.01$, and ***$P < 0.001$).

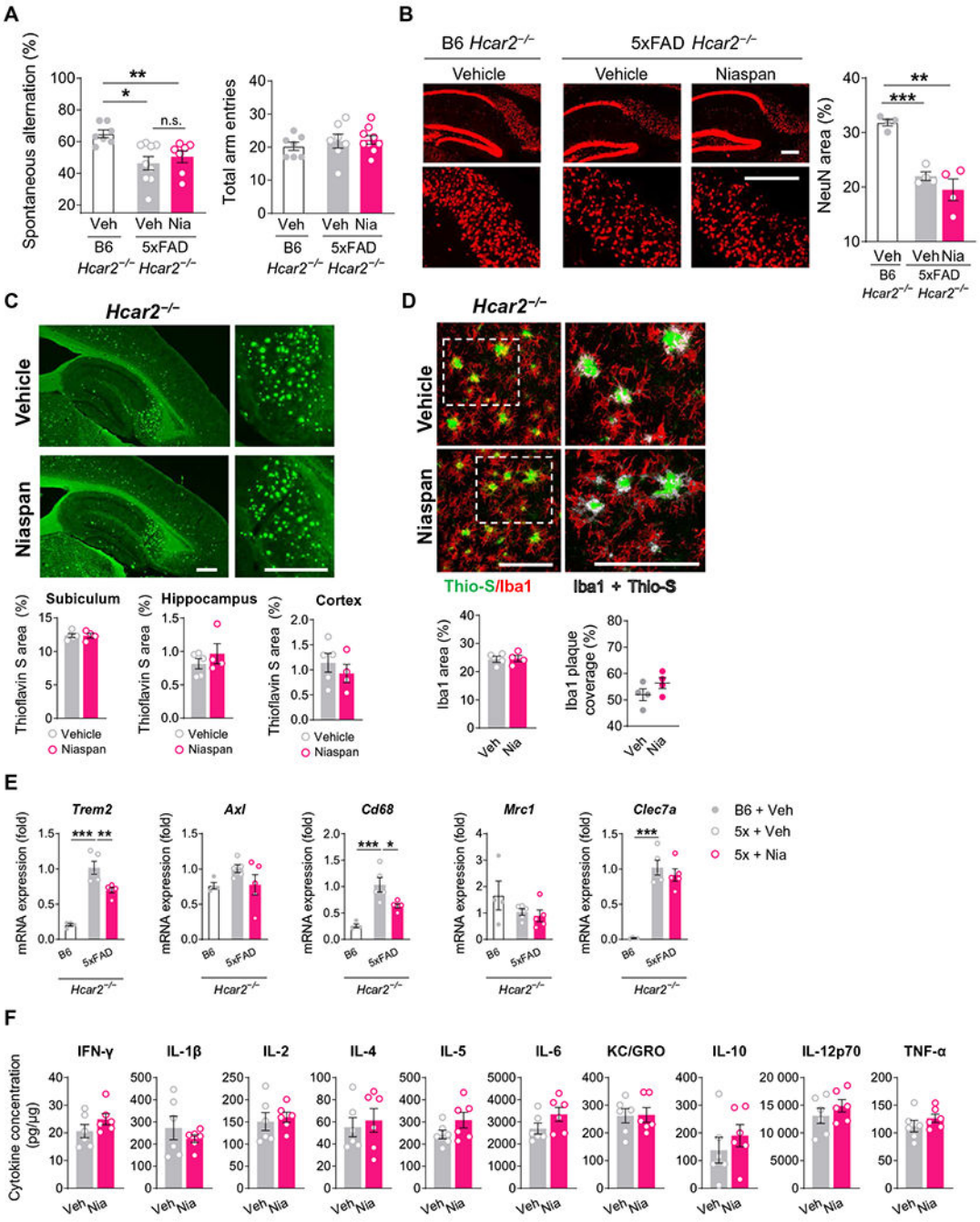

Fig. 7. Niaspan treatment does not lead to salutary effects in 5xFAD lacking *Hcar2*.

(**A**) Working memory of 6-month-old male B6 and 5xFAD *Hcar2*$^{-/-}$ mice treated with vehicle (Veh) and Niaspan (Nia) assessed by percent of spontaneous alternation in the Y-maze task. Total arms entries were also analyzed ($n = 7$ to 9 mice per group). Statistical analysis was performed by one-way ANOVA for spontaneous alternation ($P < 0.01$) and total arm entries ($P = 0.655$) followed by Tukey's post hoc test. (**B**) IHC for NeuN (neurons; red) in hippocampus of 6-month-old male B6 and 5xFAD *Hcar2*$^{-/-}$ mice treated with vehicle or Niaspan with magnification of subiculum area (bottom). Quantification of total area of

NeuN staining within the subiculum ($n = 4$ per group). Statistical analysis was performed by one-way ANOVA ($P < 0.001$) followed by Tukey's post hoc test. Scale bars, 250 μm. (**C**) IHC staining of amyloid plaques with thioflavin S and quantification of thioflavin S percent and plaque number in the subiculum, hippocampus, and cortex of 6-month-old male 5xFAD treated with vehicle and Niaspan. Subiculum (Sub) is magnified on the right ($n = 4$ per group). Statistical analysis was performed by Student's *t* test. Scale bars, 500 μm. (**D**) IHC staining for Iba1 (red) and amyloid plaques (thioflavin S; green) in the subiculum of 6-month-old male 5xFAD;*Hcar2*$^{-/-}$ mice treated with vehicle (Veh) and Niaspan (Nia). Total Iba1 area in subiculum was quantified (left graph) ($n = 4$ per group). Iba1 covarage of thioflavin S–positive plaques can be visualized by the color gray in the right IHC panel. Iba1 coverage of plaques were quantified and averaged per animal (right graph) ($n = 4$ mice and >200 plaques per group). Scale bars, 100 μm. Statistical analysis was performed by Student's *t* test. (**E**) Expression analysis by qPCR of several genes implicated in HCAR2 signaling and AD pathology in the hippocampus of male B6 and 5xFAD *Hcar2*$^{-/-}$ mice treated with vehicle and Niaspan ($n = 4$ to 5 per group). Statistical analysis was performed by one-way ANOVA ($P < 0.05$ for *Trem2, Cd68*, and *Clec7a*; $P = 0.1851$ for Axl; $P = 0.2377$ for *Mrc1*) followed by Tukey's post hoc test. (**F**) Cytokine concentration in cortical tissue of 5xFAD;*Hcar2*$^{-/-}$ mice treated with vehicle or Niaspan ($n = 6$ per group) quantified by the MSD V-PLEX Plus Proinflammatory Panel 1 Mouse Kit. Statistical analysis was performed by Student's *t* test. Data are expressed as mean values ± SEM (*$P < 0.05$, **$P < 0.01$, and ***$P < 0.001$).